J. Fluid Mech. (2008), *vol.* 613, *pp.* 1–33. © 2008 Cambridge University Press
doi:10.1017/S0022112008003236 Printed in the United Kingdom

Inviscid axisymmetric absolute instability of swirling jets

J. J. HEALEY

Department of Mathematics, Keele University, Keele, Staffs. ST5 5BG, UK
j.j.healey@keele.ac.uk

(Received 2 April 2007 and in revised form 19 June 2008)

The propagation characteristics of inviscid axisymmetric linearized disturbances to swirling jets are investigated for two families of model velocity profiles. Briggs' method is applied to dispersion relations to determine when the basic swirling jets are absolutely or convectively unstable. The method is also applied to the neutral inertial waves used by Benjamin to characterize the subcritical or supercritical nature of the flow. Although these waves are neutral, Briggs' method nonetheless indicates a qualitative change in behaviour at Benjamin's criticality condition. The first model jet has uniform axial velocity, rigid-body rotation and issues into still fluid. A known difficulty in the application of Briggs' method to the analytical dispersion relation for inviscid waves in this flow is resolved. The difficulty is that the pinch point can cross into the left half of the complex-wavenumber plane, where waves grow exponentially with radius and fail to satisfy homogeneous boundary conditions. In this paper the physical consequences of this behaviour are explained. It is shown that if the still fluid is of infinite extent in the radial direction, then the jet is convectively unstable to axisymmetric waves, but if the jet is confined by an outer cylinder concentric with the jet axis, then it becomes absolutely unstable to axisymmetric waves provided that the swirl (ratio of azimuthal to axial velocity) is large enough. This destabilizing effect of confinement occurs however large the radius of the outer cylinder. A second family of model swirling jets with smooth profiles and a finite thickness shear layer at the jet edge is also studied. The inviscid stability equations are solved numerically in this case. The results from the analytical dispersion relations are reproduced as the shear layer thickness tends to zero. However, increasing this thickness acts to destabilize the absolute instability of axisymmetric waves, apparently due to the centrifugal instability present in the shear layer. It is suggested that the transition from convective to absolute instability could be associated with the onset of an unsteady vortex breakdown. The swirl required to produce this transition can be either greater, or less, than the swirl required to produce the transition from supercritical to subcritical flow, depending on the details of the basic velocity profiles. A codimension-two point in parameter space can exist where the unsteady bifurcation associated with the convective–absolute transition coincides with the steady bifurcation associated with the supercritical–subcritical transition. Such codimension-two points can control a rich variety of nonlinear dynamical behaviour.

1. Introduction

This paper is concerned with the instabilities of swirling jets. In particular, the propagation characteristics of inviscid unstable axisymmetric waves are determined.

https://doi.org/10.1017/S0022112008003236 Published online by Cambridge University Press

Swirling jets arise in diverse technological applications. The swirl might be introduced as part of a flow-control strategy, or could occur naturally in the flow. Swirling wakes, like trailing wing tip vorticities, are another special case of a family of jet/wake flows, which can have varying degrees of external axial co-flow, or counter-flow, relative to the axial velocity of the vortex core, and which can be studied using the same methods as presented here. Another related family of flows, amenable to our approach, has a swirling jet issuing into a swirling outer flow, as in Ivanic, Foucault & Pecheux (2003). The present investigation is motivated by the phenomenon of vortex breakdown of swirling jets in which an axisymmetric bubble of recirculating fluid, with front and rear stagnation points, spontaneously appears in the fluid. This bubble acts like a bluff body, and the wake-like flow behind it can break down via helical modes.

Vortex breakdown was first observed in the flow over delta wings in the late 1950s. Harvey (1962) showed how it could be conveniently studied in swirling flows in pipes, and many remarkable flow visualizations of vortex breakdown can be seen in Sarpkaya (1971). Squire (1960) and Harvey (1960) suggested that it arises by a similar mechanism to that which produces hydraulic jumps in the flow of shallow water. Benjamin (1962) developed a theoretical framework for describing vortex breakdown, like a hydraulic jump, as the transition region connecting an upstream supercritical flow, where all disturbances travel downstream only, to a downstream subcritical flow, where disturbances can travel upstream and downstream. Benjamin was careful to distinguish his theory from rival theories that proposed that vortex breakdown is the outcome of a hydrodynamic instability of the basic swirling jet flow. Benjamin argued that the supercritical or subcritical state of the flow is determined by the propagation properties of neutral inviscid inertial waves, and presented a criterion for the existence of a linearized wave with zero phase velocity, which separates supercritical from subcritical flows.

Tsai & Widnall (1980) extended these ideas by including non-axisymmetric waves, arbitrary axial wavenumbers and by considering the group velocity for neutral waves. In the long-wave limit the neutral waves are non-dispersive and the group velocity coincides with the phase velocity used by Benjamin. However, the generalization to include the propagation properties of instability waves requires the use of Briggs' (1964) method to distinguish between convectively unstable flows, where all disturbances travel downstream, as in supercritical flow, and absolutely unstable flows, where disturbances travel upstream and downstream, as in subcritical flow. Gaster (1968) independently recognized the importance of the distinction between absolute and convective instability in shear layers, and these ideas were taken up again in fluid flows by Huerre & Monkewitz (1985); see also Huerre & Monkewitz (1990).

Absolute instability is identified by considering the wave packet response to an impulsive disturbance to an otherwise undisturbed basic flow. This response can be obtained by evaluating inverse Fourier–Laplace-type transforms over frequencies and wavenumbers. The frequency (Laplace-type) transform is evaluated by placing the integration path above singularities in the complex-frequency plane to respect the principle of causality, i.e. to ensure zero response before introduction of the impulse, then closing the path in the lower half-plane allows residue theory to be used. The problem is thus reduced to an integral in the wavenumber plane, and the integration path is placed on the real axis. At large times this integral can be estimated by deforming the integration path to cross the highest saddle point whose valleys contain the real axis. This dominant saddle is the pinch point of Briggs' method. If the imaginary part of the frequency at the pinch point is positive in the rest frame

https://doi.org/10.1017/S0022112008003236 Published online by Cambridge University Press

then the flow is absolutely unstable. For the axisymmetric jets considered here, it is the axial wavenumber plane that is of interest; the azimuthal wavenumber is an integer.

A number of authors have investigated the possibility of relating the onset of vortex breakdown to the onset of a transition of the jet from a convectively unstable state to an absolutely unstable state, and this is the line of research we have sought to extend in this paper. After all, it seems reasonable that if a jet supports unstable waves, then it may be their propagation characteristics that determine the appearance of vortex breakdown, because they are expected to dominate the flow field. However, if the unstable waves are only convectively unstable, but the neutral waves propagate upstream, then these neutral waves could produce breakdown. Briggs' method incorporates all modes of the dispersion relation, stable, neutral and unstable, so Benjamin's criticality condition, based on neutral inertial waves, can also be investigated from the perspective of Briggs' method.

However, we shall show that the unstable waves that are usually the focus of attention in absolute instability calculations lie on a different Riemann surface to that of the neutral inertial waves that give rise to Benjamin's criticality condition. Therefore, spatio-temporal studies restricted to the most unstable waves fail to capture the supercritical–subcritical transition.

Our new absolute instability results for swirling jets will be placed in the context of earlier investigations into the steady bifurcations associated with Benjamin's criticality condition. A review of this work on criticality, previous work on the absolute instability of these flows, and some recent developments in the theory of absolute and convective instabilities that are particularly relevant to swirling jets, is presented in § 2. Discussion of the steady bifurcations associated with Benjamin's criticality condition is given in § 2.1. These bifurcations give rise to axially periodic states and solitary waves. The solitary waves can enclose a region of reverse flow and have been proposed as an explanation for steady axisymmetric vortex breakdown states. A difficulty often encountered in the application of Brigg's method to swirling jets is the migration of the dominant saddle point (pinch point) into the left half of the complex-wavenumber plane. Examples of this behaviour are discussed in § 2.2. These left half-plane modes grow exponentially with the radial coordinate and seem not to satisfy homogeneous boundary conditions. However, the author has recently discovered the physical interpretation of this behaviour in the context of the rotating-disk boundary layer; these developments are explained in § 2.3. An important consequence is that such flows are sensitive to confinement, even when the confining boundary is far from the shear layer. In particular, confinement can enhance, or even create, absolute instability in these flows. These observations are interesting in the context of vortex breakdown, because flows confined in pipes are often studied in experiments since they produce more robust breakdown phenomena than unconfined flows.

The linearized inviscid stability equations for axisymmetric disturbances to a columnar vortex are presented in § 3. In § 4 we consider the model swirling jet flow studied by Lim & Redekopp (1998), and Gallaire & Chomaz (2003*a*), in which a jet in rigid-body rotation, and with uniform axial velocity, issues into still fluid. This inviscid flow with discontinuous velocity profiles admits an analytical dispersion relation. It is shown that confinement can create an absolute instability of axisymmetric waves. Benjamin's criticality condition is studied from the perspective of Brigg's method, and it is found that for this flow the convective–absolute transition takes place at a higher swirl (a ratio of azimuthal to axial velocity) than that for the supercritical–subcritical

https://doi.org/10.1017/S0022112008003236 Published online by Cambridge University Press

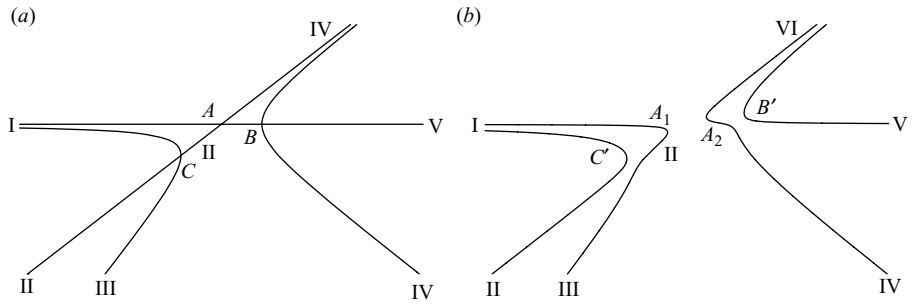


FIGURE 1. Bifurcation diagrams of steady solutions with swirl on horizontal axis and a measure of axial velocity on vertical axis. Branch I, supercritical primary vortex; branch II, subcritical conjugate vortex; branch III, solitary waves on supercritical primary vortex; branch IV, solitary waves on supercritical conjugate vortex; branch V, subcritical primary vortex; branch VI, supercritical conjugate vortex; A, transcritical bifurcation at Benjamin's criticality condition; B and C, pitchfork bifurcations creating standing waves on subcritical branches. (a) Summary of results of Leibovich & Kribus (1990), including the proposed pitchfork bifurcation C, for a pipe of fixed finite length L. (b) Possible unfolding of (a) created by including small viscosity, where A_1, A_2, B' and C' are limit points replacing the bifurcation points A, B and C.

transition (except in a very narrow range of the confinement parameter). A new model swirling jet with smooth velocity profiles that approaches Lim & Redekopp's model as shear layers at the jet edge are reduced in thickness is presented and analysed in § 5. Thickening the shear layers at the jet edge is found to promote axisymmetric absolute instability, via centrifugal instability, while at the same time tending to suppress the transition to subcritical flow. Confinement has little effect on the supercritical–subcritical transition, but enhances the absolute instability. Thus, depending on the shear layer thickness, and the level of confinement, a supercritical and convectively unstable flow can become either subcritical or absolutely unstable as the swirl parameter is increased. These findings are discussed in § 6.

2. Review

2.1. *Supercritical–subcritical transition of swirling jets*

Leibovich & Kribus (1990) studied the steady bifurcations of inviscid columnar vortices in a pipe associated with change in criticality as swirl is varied. They showed that the first bifurcation encountered as the swirl parameter is increased is a transcritical bifurcation creating new columnar states that are conjugate to the original state in the sense used by Benjamin: they are subcritical when the primary (specifying) columnar vortex is supercritical and they are supercritical when the primary vortex is subcritical: see figure 1(a). This transcritical bifurcation occurs at the swirl level given by Benjamin's criticality condition and is marked A in figure 1(a). For a fixed-length pipe, there is a pitchfork bifurcation from the subcritical primary vortex, marked B in figure 1(a), at which small amplitude standing waves appear. These waves have axial wavelength equal to the length of the pipe, L, which is made dimensionless with pipe radius, and as the swirl is increased, the wave amplitude increases. The wave crests become flatter, and the troughs deeper and sharper, as their amplitude is increased, and the waves evolve in this manner into solitary waves like those found by Benjamin (1967). Further pitchfork bifurcations from the subcritical primary vortex occur with increasing swirl (not shown here), producing standing waves with wavelengths L/m

https://doi.org/10.1017/S0022112008003236 Published online by Cambridge University Press

for integer m, and these too evolve into solitary waves. The velocity profiles at the flat crests approach those of the supercritical conjugate branch. These solitary waves therefore ride on the supercritical conjugate branch, but originate from standing waves appearing at pitchfork bifurcations on the subcritical primary branch. The upper branch of each pitchfork corresponds to an axial velocity measurement at a wave crest, and the lower branch to a measurement at a wave trough. Reversed flow occurs at troughs when the swirl is large enough, which is reminiscent of vortex breakdown.

Leibovich & Kribus also showed that as L increases, the amplitude required to produce solitary waves reduces, and as $L \to \infty$, weakly nonlinear solitary waves exist close to criticality. These are the solitary waves first found by Benjamin (1967) and they ride on the supercritical primary vortex; they are labelled III in figure 1. However, at fixed L, branch III cannot be continued towards the transcritical bifurcation point A in the way depicted in figure 19 of Beran & Culick (1992), because, as discussed in § 3.2 of Leibovich & Kribus, when the wave amplitude is sufficiently small (less than $O(L^{-1/2})$), the solitary wave theory becomes invalid. We suggest instead that standing waves should appear at a pitchfork bifurcation, marked C in figure 1(a), at a fixed finite L, which then evolve into solitary waves further from C, marked III. Therefore, these solitary waves ride on the primary supercritical branch I, but arise at a pitchfork bifurcation point, C, on the subcritical conjugate branch II.

However, comparison between these inviscid results and experiments on, or numerical simulations of, viscous fluids is not straightforward. The transcritical and pitchfork bifurcations shown in figure 1(a) are structurally unstable, i.e. arbitrarily small generic imperfections to the system will cause the solution branches to connect to one another in a qualitatively different arrangement. See Benjamin (1978) for a discussion of how perturbations to these bifurcations can produce new arrangements of solution branches in the context of hydrodynamic stability problems and Benjamin & Mullin (1981) for examples of this phenomenon in the Taylor–Couette experiment.

Wang & Rusak (1997a) have shown in a small-viscosity perturbation theory that the transcritical bifurcation, A, in the inviscid problem breaks apart to give two limit points: one, labelled A_1 in figure 1(b), connects the supercritical primary vortex branch I to the subcritical conjugate vortex branch II, and the other, labelled A_2, connects the supercritical conjugate vortex branch VI to the subcritical primary vortex branch V. Imperfections will also disconnect the pitchfork bifurcations, e.g. as in figure 1(b), leading to the limit points B' and C'. Thus, while figure 1(a) describes the behaviour arising at a change in criticality of an inviscid parallel vortex, our suggested figure 1(b) accounts for the symmetry-breaking imperfections present in experiments and simulations of viscous fluids.

Beran & Culick (1992) obtained numerical solutions to the steady axisymmetric viscous equations for swirling flow in a pipe. Numerical continuation methods were used to follow steady solutions around limit points. At low Reynolds numbers the minimum centreline axial velocity reduces smoothly as the swirl is increased, but for higher Reynolds numbers a limit point is encountered, which was associated with that at A_1, i.e. due to the disconnection of the transcritical bifurcation that appears at criticality in the inviscid theory. When the solution is followed around this limit point, they found that standing axially periodic waves gradually appear, which become progressively more like solitary waves: see figures 20 and 22 of Beran & Culick (1992). These figures correspond closely to our figure 1(b) where branch I connects to branch II at the limit point A_1, and then evolves into the solitary waves of branch III via standing axially periodic waves that emerge near the perturbed

https://doi.org/10.1017/S0022112008003236 Published online by Cambridge University Press

pitchfork bifurcation C'. These solitary waves develop regions of reversed axial flow, as in vortex breakdown, and as in the inviscid theory of Leibovich & Kribus (1990).

Beran & Culick (1992) also discovered a second limit point causing branch III to bend back towards the right of the diagram. Wang & Rusak (1997*b*) found a similar limit point in their inviscid theory. This pair of limit points gives rise to hysteresis. Beran & Culick proposed that increasing the swirl above its value at A_1 leads to an abrupt transition to a vortex breakdown state with reversed flow. Lopez (1994) carried out an axisymmetric time-dependent simulation of swirling flow in a pipe and confirmed this scenario. Wang & Rusak (1996) have shown that the associated loss of stability of the steady solutions at A, or A_1, is a feature of flow in a finite-length pipe, even though the solutions would be neutrally stable for an infinitely long pipe of inviscid fluid. Gallaire & Chomaz (2004) have shown how the boundary conditions in a finite-length pipe can supply energy to the disturbances and thus drive the instability. Therefore, in a finite-length pipe, there is an exchange of stability as well as a supercritical–subcritical transition at the transcritical bifurcation A in figure 1(*a*).

In addition to these steady solutions, unsteady axisymmetric solutions have been observed. Escudier (1984) observed such solutions in an experimental investigation, Lopez (1994) found them in the time-dependent axisymmetric numerical simulations referred to above, and Ruith *et al.* (2003) obtained these solutions when non-axisymmetric disturbances were switched off in their simulations. Ruith *et al.* found that their oscillating axisymmetric solutions were unstable to non-axisymmetric disturbances, but Escudier's experimental observations show that these unsteady solutions can be stable. Liang & Maxworthy (2005) observed unsteady axisymmetric vortex breakdown in experiments at swirls just below that at which a steady non-axisymmetric vortex breakdown occurs.

We have discussed how the steady bifurcations of an inviscid primary columnar vortex originate from Benjamin's supercritical–subcritical transition. This criticality condition is associated with the appearance of a zero-wavenumber, zero-phase-velocity, solution of the dispersion relation for neutral inertial waves. We suggest that the appearance of unsteady axisymmetric solutions could be associated with the existence of a convective–absolute instability transition involving waves of finite wavenumber and finite frequency.

The following review of absolute instability investigations of swirling jets shows that while absolute instability has often been demonstrated for non-axisymmetric waves, the calculation of absolute instability of axisymmetric waves has proved much more problematic. This is due to a tendency of the pinch point of Briggs' method (the dominant saddle point in a large-time solution to the initial-value problem) to move, when the swirl is increased, into the left half of the complex-wavenumber plane, where solutions grow exponentially in the radial direction. This tendency is also present in the non-axisymmetric calculations. The interpretation of this behaviour, and its consequences for the effect of confinement, will be reviewed in § 2.3, and these insights pave the way for the present investigation of axisymmetric absolute instability, but would apply equally to non-axisymmetric calculations.

2.2. *Convective–absolute transition of swirling jets*

Previous studies of the absolute instability of swirling jets and wakes retained an external-flow parameter, different values of which correspond to different velocities of the frame of reference. A frame of reference can always be found that will make any unstable flow absolutely unstable, though usually a particular frame, the laboratory

https://doi.org/10.1017/S0022112008003236 Published online by Cambridge University Press

frame, has special significance. In this paper, we shall confine our attention to the case of a swirling jet issuing into an otherwise still body of fluid, i.e. with no external flow, as in, for example, the experiments by Billant, Chomaz & Huerre (1998) and Liang & Maxworthy (2005).

Lim & Redekopp (1998) looked at the inviscid instability of axisymmetric waves added to a model swirling jet with a core in rigid-body rotation and with uniform axial flow in the core. This basic flow has an analytical dispersion relation. With no swirl (the swirl is the ratio of the azimuthal velocity scale to the axial velocity scale) this jet is convectively unstable. As the swirl increases they found that although the (negative) imaginary part of the frequency at the pinch point increases, the pinch point crosses into the left half of the complex-wavenumber plane while the imaginary part of this frequency is still negative. Far from the jet core, waves either grow or decay exponentially with the radial coordinate. Branch cuts are placed along the imaginary axes of the wavenumber plane so that only solutions that decay in the radial direction are considered; these solutions satisfy homogeneous boundary conditions. If the pinch point is followed into the left half-plane, then a branch cut has to be moved from the imaginary axis, and the solution at the pinch point then grows exponentially in the radial direction. Such behaviour seemed unphysical and was not considered further. However, Lim & Redekopp also noted that in the corresponding confined problem, where the jet is surrounded by a coaxial cylinder of larger radius than that of the jet, reducing the radius of this cylinder also increases the imaginary part of the frequency at the pinch point, though it remained negative for the parameter values that they considered. Nonetheless, Lim & Redekopp showed that reducing the density of the jet core relative to the external fluid does produce an axisymmetric inviscid absolute instability in agreement with results of Monkewitz & Sohn (1988), who looked at the zero-swirl case.

Loiseleux, Chomaz & Huerre (1998) considered the inviscid absolute instability of the Rankine vortex with uniform axial flow in its core. The Rankine vortex has a continuous azimuthal velocity profile with a core in rigid-body rotation surrounded by a potential vortex; the axial velocity is discontinuous at the jet edge. An analytical dispersion can be written down for this problem too. In fact, Lim & Redekopp considered a model with a parameter that included this flow as one limit, and the flow with no external potential vortex in another limit; Lim & Redekopp found the external potential vortex to have a stabilizing influence on the pinch point for axisymmetric waves. Loiseleux *et al.* explored the spatio-temporal behaviour of waves with non-zero azimuthal wavenumbers, and their figure 17(*c*) shows that these pinch-points can also cross into the left half of the wavenumber plane, but this feature was not commented upon. Loiseleux *et al.* also found that matters could be further complicated by the presence of more than one saddle point, and changes in dominance between saddle points.

Olendraru *et al.* (1999) considered the inviscid absolute instability of the Batchelor vortex, which has smooth axial and azimuthal velocity profiles: see Batchelor (1964). The Batchelor vortex has fluid in rigid-body rotation at its axis, and asymptotes to a potential vortex far from the axis; it has been used as a model for wing tip trailing vorticies, and also for the swirling flows upstream and downstream of a vortex breakdown. Numerical methods were used to solve the stability equations. The axisymmetric waves are stable. Figure 8(*a*) of their paper shows that the pinch point for the azimuthal wavenumber $m = -1$ reaches the imaginary wavenumber axis at swirl $q = 1.3$, and would cross into the left half of the wavenumber plane for larger swirl, but this was not discussed. Neutral curves for the onset of absolute instability

https://doi.org/10.1017/S0022112008003236 Published online by Cambridge University Press

in the external-flow parameter versus swirl plane are left incomplete at larger swirl values due to numerical difficulties.

The numerical challenges associated with obtaining inviscid stability results for the smooth Batchelor vortex, the multiple saddle points and the problem of interpreting the behaviour of pinch points that cross into the left-half wavenumber plane, motivated Delbende, Chomaz & Huerre (1998) to develop an alternative to Briggs' method for determining the absolute or convective character of the instability for the viscous version of the problem. Their method is based on carrying out a direct numerical simulation of the linearized equations for a localized disturbance to a given basic velocity profile (which does not evolve in the downstream direction). Time series analysis techniques are then applied to data from the simulation to construct an envelope for the resulting wave packet, and to estimate the growth rate of this envelope in any given frame of reference. Results were presented at one Reynolds number (the method is computationally intensive), and qualitative agreement with Olendraru *et al.*'s results was obtained. They were also able to complete Olendraru *et al.*'s neutral curves at higher swirl values. At their chosen Reynolds number the Batchelor vortex is convectively unstable for all azimuthal wavenumbers, m, in the frame with zero external axial flow for all swirl values, but only a small reverse external axial flow is needed to produce absolute instability. No light could be shed on the issue of pinch points crossing into the left-half wavenumber plane because the axial wavenumber was restricted to values greater than 0.6 (made dimensionless using the jet radius) so that the disturbance decays sufficiently rapidly in the radial direction for it to be negligible at the cross-stream edge of the computational domain where boundary conditions are applied.

Ruith *et al.* (2003) carried out direct numerical simulations using as in-flow conditions the two-parameter columnar swirling-jet model of Grabowski & Berger (1976), which has continuous azimuthal and axial velocity profiles with polynomial radial dependence inside the core, and outside the core there is a potential vortex and uniform axial flow. In simulations at lower values of the Reynolds number Ruith *et al.* found a steady axisymmetric vortex breakdown; as the Reynolds number increases, the wake-like flow behind this breakdown bubble becomes unstable to self-sustained helical modes with azimuthal wavenumbers of $m = -1$ or $m = -2$ dominating. They also found that if non-axisymmetric disturbances are suppressed then at higher Reynolds numbers the axisymmetric vortex breakdown bubble becomes time-periodic, as in the experiments by Escudier (1984). Ruith *et al.* modelled the axisymmetric flow downstream of the axisymmetric vortex breakdown bubble by Batchelor vorticies with appropriate swirl and external-flow parameters, and used Delbende *et al.* (1998)'s results to show that these profiles become absolutely unstable to $m = -1$ and $m = -2$ helical waves. Global mode theories reviewed in Huerre & Monkewitz (1990) indicate that if there exists a large enough streamwise extent of flow that is (locally) absolutely unstable, then an unstable linear global mode can exist. Ruith *et al.* argued that increasing the Reynolds number extends the locally absolutely unstable domain of the wake behind the axisymmetric breakdown bubble, thus leading to an unstable helical linear global mode that, when its amplitude has been saturated by nonlinearity, accounts for the spiral behaviour seen in their simulations, and reported in experiments.

This picture is in agreement with the scenario proposed by Escudier, Bornstein & Maxworthy (1982): the fundamental vortex breakdown structure is the axisymmetric bubble, which has supercritical flow upstream and subcritical flow downstream. The helical breakdown modes are then the result of helical instabilities of the wake-like

https://doi.org/10.1017/S0022112008003236 Published online by Cambridge University Press

flow downstream of the axisymmetric bubble, but the bubble itself was argued not to be due to an instability. However, the work discussed in § 2.1 suggests that the abrupt appearance of reversed flow can be associated with the loss of stability at the limit point A_1 found by Beran & Culick (1992) and Lopez (1994), and which can be related to Benjamin's criticality condition through Wang & Rusak (1997*a*)'s unfolding of the transcritical bifurcation, A, found by Leibovich & Kribus (1990) in the underlying inviscid problem: see figure 1.

Irrespective of the role of instability in the genesis of axisymmetric vortex breakdown, Gallaire *et al.* (2006) have further clarified the role of absolute instability in generating helical modes downstream of the axisymmetric bubble. They took Ruith *et al.*'s axisymmetric vortex breakdown flow as a basic state, and determined the local stability of velocity profiles at a series of downstream locations using the method of Delbende *et al.* (1998). They showed that the self-sustained helical modes found in Ruith *et al.*'s simulations can be related to steep-fronted nonlinear global modes triggered at a streamwise location where there is a transition from convective to absolute instability, as described by Couairon & Chomaz (1999) and Pier, Huerre & Chomaz (2001).

While progress has been made in understanding the helical modes of vortex breakdown in terms of an absolute instability of non-axisymmetric waves, we are only aware of one study showing axisymmetric absolute instability of a swirling jet which has no axial flow outside the jet core. Loiseleux, Delbende & Huerre (2000) investigated a model jet in which the core has uniform axial flow and constant circulation, and which has a different constant circulation, and no axial flow, outside the core. The resulting singularity in azimuthal velocity at the jet axis is clearly unphysical, but an analytical dispersion relation can be written down for inviscid linearized waves, and the effects of increasing and decreasing jumps in circulation were investigated. They found that increasing the magnitude of the circulation jump enhances absolute instability, but which modes will be destabilized depends on the sign of the jump, with the axisymmetric mode preferred when the jump is centrifugally destabilizing, and a large negative azimuthal wavenumber preferred when the jump is centrifugally stabilizing.

However, axisymmetric absolute instability has not been found in more realistic swirling-jet velocity profiles with finite velocity fields, the difficulty being that in such flows the pinch point moves into the left half of the wavenumber plane as the swirl increases. A similar tendency can occur for non-axisymmetric waves, but these waves can become absolutely unstable before the pinch point reaches the imaginary wavenumber axis. A pinch point behaving in this way produces waves that decay more and more slowly in the radial direction, so this behaviour also implies difficulties for numerical simulations because it means that the computational domain must be increased substantially in the radial direction. We now review the new developments in the theory of absolute and convective instabilities that address this issue, provide the physical interpretation of modes in the left half-plane, and describe the counter-intuitive destabilizing effect of confinement in such problems.

2.3. *Left-half-wavenumber-plane modes*

In fact, the problem of the pinch point crossing into the left-half wavenumber plane is not just a peculiarity of swirling jet flows. It has also been observed in a study of a smooth plane mixing layer (see Huerre & Monkewitz 1985), and in plane jets and wakes with variable density and piecewise constant velocity profiles (see figure 7 of Yu & Monkewitz 1990), figure 4 of Juniper & Candel (2003) and Juniper

https://doi.org/10.1017/S0022112008003236 Published online by Cambridge University Press

(2006). These occurrences were either ignored in the text (but are apparent from data in figures), or explicitly dismissed on the grounds that they are unphysical. For example, Gallaire & Chomaz (2003*a*) suggested that this apparently unphysical behaviour indicates the breakdown of validity of the basic flow model (they were investigating Lim & Redekopp's flow, which has discontinuous profiles, and therefore represents an ill-posed initial-value problem because the resulting Kelvin–Helmholtz instability amplifies arbitrarily short length scales with arbitrarily large growth rates).

However, Healey (2006*a*) showed that the pinch point of the absolute instability in the rotating-disk boundary layer becomes asymptotically close to the imaginary axis of the appropriate complex-wavenumber plane in the long-wave limit in the inviscid stability problem. The basic flow was von Kármán's similarity profile, which is an exact solution of the Navier–Stokes equations. The stability results were obtained analytically using matched asymptotic expansions and are a self-consistent approximation to the Navier–Stokes equation. It was confirmed that they give accurate quantitative predictions when compared with numerical solutions to the stability equations. Therefore, pinch points approaching the left half of the complex-wavenumber plane are genuine features of spatio-temporal hydrodynamic stability investigations, and require physical interpretation.

A global investigation of the wavenumber plane was needed, which was beyond the scope of the long-wave theory described above. This was carried out by Healey (2006*b*). It was discovered that there are unstable modes that grow exponentially in the wall-normal direction in the rotating-disk boundary layer when the wavenumbers are small enough. These modes are efficiently described using parts of the dispersion relation continued into the left half-plane. Although these roots of the dispersion relation grow exponentially, and are indeed unbounded in the wall-normal direction, and therefore do not satisfy homogeneous boundary conditions, the physical disturbance produced by an initial-value problem does always satisfy homogeneous boundary conditions. This is because the flow field is initially undisturbed, and the disturbance created by forcing at the wall only propagates in the wall-normal direction at finite velocities. The wall-normal propagation velocities can be predicted using a saddle-point method incorporating terms corresponding to propagation in both the streamwise and wall-normal directions (by combining the 'wavy' complex exponential with the exponential form of the eigenfunction taken by the disturbance where the basic flow is uniform). These saddle points can exist in either the left- or right-hand halves of the complex plane, but their large-time predictions of wall-normal exponential growth and propagation agree well with numerical evaluations of the inverse transforms calculated using integration paths that pass only over sheets of the dispersion relation that decay exponentially in the wall-normal direction. The part of the dispersion relation that controls the wall-normal growth and propagation has also been described by long-wave theory: see Healey (2005).

The physical behaviour of wall-normal growth and propagation associated with a pinch point crossing into the left half-plane is sensitive to how the flow is confined in the wall-normal direction. One can normally assume that if the boundary to the flow in the crossflow direction is far enough away, then the exponential decay of disturbances in the crossflow direction allows the flow to be treated as unconfined in that direction. However, this is not the case for flows that generate exponential growth in the crossflow direction: no matter how far away the outer boundary is placed, it still quantitatively, and qualitatively, affects the spatio-temporal stability properties of the flow, as first shown by Healey (2007). Disturbances grow in the

https://doi.org/10.1017/S0022112008003236 Published online by Cambridge University Press

wall-normal direction in accordance with the unconfined-flow theory until they reach the outer boundary. There is then a period of reflections of the disturbance between the boundary layer plate and the outer plate while a standing wave is established. At large times, when the outer plate is far from the boundary layer, this standing wave has absolute instability growth rate equal to the maximum growth rate of the wall-normal propagating disturbance of the unconfined flow, and is given by a local maximum of the imaginary part of the frequency evaluated along the imaginary wavenumber axis. Moving the outer plate closer to the shear layer actually increases the absolute instability growth rate (unless the outer plate becomes very close to the shear layer). Therefore, confinement can, in principle, create an absolutely unstable flow from one that would only be convectively unstable when unconfined. These conclusions all follow from the fact that confining a flow is a singular perturbation since the continuous spectrum arising from a branch cut of the dispersion relation for the unconfined flow is replaced by an infinite discrete spectrum for the confined flow, and Healey (2007) has shown how this leads to infinitely many new saddle points being created, one of which can form the new pinch point.

The results of Lim & Redekopp (1998), Juniper & Candel (2003) and Juniper (2006) concerning the effect of confinement in problems with pinch points approaching, or crossing into, the left half-plane are all consistent with the framework developed in Healey (2006*b*) and Healey (2007), though the implications of a pinch point entering the left half-plane, and the expected consequences of confinement on the absolute instabilities, were not understood at the time. Juniper (2007) has re-examined his results concerning left half-plane modes in the light of these findings and reproduced in detail in the context of plane wakes and jets of variable density the scenarios described in Healey (2006*b*) and Healey (2007) for the rotating-disk boundary layer.

In the context of swirling jets, a pinch point with negative imaginary part of frequency crossing the imaginary axial wavenumber axis has no immediate physical consequence, but if, as the swirl is increased, a spatial branch with positive imaginary part of frequency follows the pinch point into the left half-plane, then a convective instability with exponential growth in the radial direction occurs, and an impulsive disturbance will generate a radially propagating wave packet that travels away from the jet, growing in amplitude as it goes. If the surrounding fluid is not of infinite extent, then a standing wave will eventually be established after the wave packet has reached the confining boundary. This standing wave will be absolutely unstable even though the unconfined flow is only convectively unstable. In the following sections we show that this behaviour in the wavenumber plane does occur for model swirling jets.

3. Governing equations

In this paper attention is restricted to axisymmetric waves. The dimensional equations of motion for axisymmetric incompressible inviscid flow in cylindrical coordinates are

$$\frac{1}{r_*}\frac{\partial(r_* u_*)}{\partial r_*} + \frac{\partial w_*}{\partial z_*} = 0, \tag{3.1a}$$

$$\frac{\partial u_*}{\partial t_*} + u_*\frac{\partial u_*}{\partial r_*} + w_*\frac{\partial u_*}{\partial z_*} - \frac{v_*^2}{r_*} = -\frac{1}{\rho_*}\frac{\partial p_*}{\partial r_*}, \tag{3.1b}$$

https://doi.org/10.1017/S0022112008003236 Published online by Cambridge University Press

$$\frac{\partial v_*}{\partial t_*} + u_*\frac{\partial v_*}{\partial r_*} + w_*\frac{\partial v_*}{\partial z_*} + \frac{u_* v_*}{r_*} = 0, \tag{3.1c}$$

$$\frac{\partial w_*}{\partial t_*} + u_*\frac{\partial w_*}{\partial r_*} + w_*\frac{\partial w_*}{\partial z_*} = -\frac{1}{\rho_*}\frac{\partial p_*}{\partial z_*}, \tag{3.1d}$$

where the radial and axial coordinates are r_* and z_* respectively, time is t_* and ρ_* is the density of the fluid. The velocities in the radial, azimuthal and axial directions are u_*, v_* and w_* respectively and the pressure is p_*. Lengths are made dimensionless using the radius of the jet, R, velocities are made dimensionless using the axial velocity of the jet on the jet axis, U_0, and time by R/U_0. The dimensionless basic flow velocity and pressure profiles for a columnar vortex are $U(r)=0$, $V(r)$, $W(r)$ and $P(r)$, where $\partial P/\partial r = V^2/r$, and the flow field is expressed as a superposition of this basic flow and small unsteady disturbances in the form

$$u_*(r_*, z_*, t_*) = \epsilon U_0 u(r)\exp \mathrm{i}(kz - \omega t), \tag{3.2a}$$

$$v_*(r_*, z_*, t_*) = U_0 V(r) + \epsilon U_0 v(r)\exp \mathrm{i}(kz - \omega t), \tag{3.2b}$$

$$w_*(r_*, z_*, t_*) = U_0 W(r) + \epsilon U_0 w(r)\exp \mathrm{i}(kz - \omega t), \tag{3.2c}$$

$$p_*(r_*, z_*, t_*) = \rho_* U_0^2 P(r) + \epsilon \rho_* U_0^2 p(r)\exp \mathrm{i}(kz - \omega t), \tag{3.2d}$$

which, when substituted into (3.1), and linearized in the small parameter ϵ, gives

$$u' + \frac{u}{r} + \mathrm{i}kw = 0, \tag{3.3a}$$

$$-\mathrm{i}\omega u + \mathrm{i}kWu - \frac{2V}{r}v = -p', \tag{3.3b}$$

$$-\mathrm{i}\omega v + \mathrm{i}kWv + V'u + \frac{V}{r}u = 0, \tag{3.3c}$$

$$-\mathrm{i}\omega w + \mathrm{i}kWw + W'u = -\mathrm{i}kp. \tag{3.3d}$$

4. A model swirling jet with discontinuous velocity profiles

We re-examine one of the basic flows studied by Lim & Redekopp (1998) in which a jet in rigid-body rotation, and with uniform axial velocity, is surrounded by still fluid of the same density. The dimensionless basic flow is

$$V(r) = \begin{cases} Sr & \text{for} \quad 0 \leqslant r \leqslant 1, \\ 0 & \text{for} \quad r > 1, \end{cases} \qquad W(r) = \begin{cases} 1 & \text{for} \quad 0 \leqslant r \leqslant 1, \\ 0 & \text{for} \quad r > 1. \end{cases} \tag{4.1a, b}$$

The swirl, $S = \Omega R/U_0$, measures the azimuthal velocity at the jet edge relative to the axial velocity, where Ω is the angular velocity of the jet. This basic flow is a simple model for the experiments of Billant *et al.* (1998) and Liang & Maxworthy (2005).

Substituting (4.1) into (3.3) and eliminating u, v and w for $0 \leqslant r \leqslant 1$ gives

$$p_1'' + \frac{p_1'}{r} + k^2\left[\frac{4S^2}{(\omega - k)^2} - 1\right]p_1 = 0, \tag{4.2}$$

where the subscript '1' denotes a variable in the core of the jet. The solution that is regular at the jet axis is

$$p_1 = J_0(\beta r), \tag{4.3}$$

where

$$\beta^2 = k^2\left[\frac{4S^2}{(\omega - k)^2} - 1\right] \tag{4.4}$$

https://doi.org/10.1017/S0022112008003236 Published online by Cambridge University Press

and J_m is the order-m Bessel function of the first kind (the solution has been normalized so that the arbitrary multiplicative constant is unity); the choice of square root in calculating β is irrelevant because J_0 is an even function, see (A 2) in the Appendix. The radial component of the disturbance, required later, is recovered from

$$u_1 = \frac{\mathrm{i}k^2}{(\omega - k)\beta^2} p_1'. \tag{4.5}$$

Substituting (4.1) into (3.3) and eliminating u, v and w for $r > 1$ gives

$$p_2'' + \frac{p_2'}{r} - k^2 p_2 = 0, \tag{4.6}$$

where the subscript '2' denotes a variable outside the core of the jet. The solution to (4.6) depends on the choice of outer boundary condition, i.e. on whether the flow is confined or unconfined in the radial direction.

4.1. *Unconfined flow*

When the flow is radially unconfined, the solution satisfying homogeneous boundary conditions, i.e. that decays exponentially as $r \to \infty$, is

$$p_2 = AK_0(\sqrt{k^2}r), \tag{4.7}$$

where A is a constant of integration, K_m is the order-m modified Bessel function of the second kind and the square-root has positive real part, which implies branch-cuts on the imaginary axes of the complex k-plane. The radial component of the disturbance, required later, is recovered from

$$u_2 = -\frac{\mathrm{i}}{\omega} p_2'. \tag{4.8}$$

The solutions in the core are matched to those outside the core by satisfying two jump conditions, which leads to the dispersion relation: see Drazin & Reid (1981). The kinematic condition requires the interface to move with the radial velocity in each region; it leads to

$$\frac{u_1(1)}{\omega - k} = \frac{u_2(1)}{\omega}. \tag{4.9}$$

The dynamic condition requires continuity of pressure across the interface; it leads to

$$p_2(1) = p_1(1) + \frac{\mathrm{i}S^2}{\omega - k} u_1(1), \tag{4.10}$$

where the second term on the right-hand side of (4.10) is due to centrifugal effects.

Substituting (4.3), (4.5), (4.7) and (4.8) into (4.9) and (4.10) and eliminating the constant A produces the dispersion relation for axisymmetric waves in the unconfined swirling jet:

$$0 = k^2 S^2 + \beta(\omega - k)^2 \frac{J_0(\beta)}{J_1(\beta)} + \omega^2 \sqrt{k^2} \frac{K_0(\sqrt{k^2})}{K_1(\sqrt{k^2})}. \tag{4.11}$$

See Lim & Redekopp (1998) for the dispersion relation with non-zero uniform axial flow, and a potential vortex, outside the core, and see Gallaire & Chomaz (2003*a*) for the dispersion relation for non-zero azimuthal wavenumbers for this more general outer flow.

Figure 3 of Lim & Redekopp (1998) shows the arrangement of spatial branches (contours of constant Im(ω)) for roots of (4.11) in the complex k-plane for $S = 0$.

https://doi.org/10.1017/S0022112008003236 Published online by Cambridge University Press

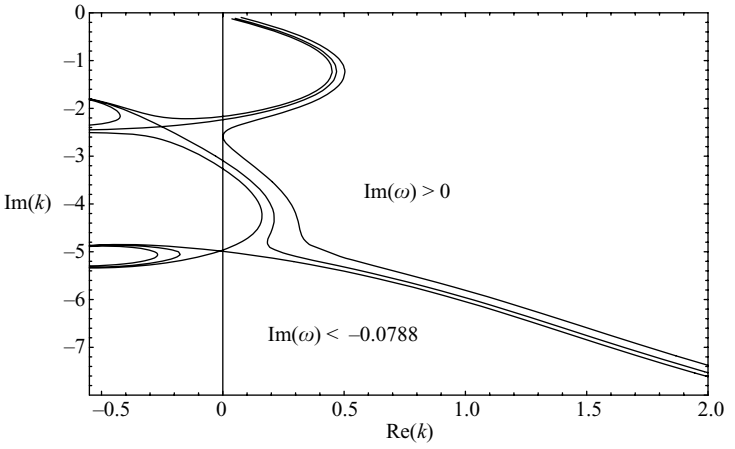


FIGURE 2. Contours of constant $\mathrm{Im}(\omega)$ in the complex k-plane for the dispersion relation for the unconfined jet (4.11) for $S = 2.882$. Contours are at $\mathrm{Im}(\omega) = -0.0788$, -0.05074 and 0. This flow is convectively unstable so the integration path can be placed in the $\mathrm{Im}(\omega) < 0$ region, i.e. to the left of the $\mathrm{Im}(\omega) = 0$ contour, starting along the negative real k-axis and leaving the diagram in the lower-right quadrant of the complex k-plane. The dominant saddle point (pinch point) lies at $k \approx -0.2514 - 2.382\mathrm{i}$, at which $\omega \approx 3.463 - 0.05074\mathrm{i}$; the other saddle point lies at $k \approx -0.01014 - 4.984\mathrm{i}$, at which $\omega \approx 4.704 - 0.07880\mathrm{i}$. The branch cut originally placed on the imaginary k-axis has been removed so that solutions with $\mathrm{Re}(k) < 0$ grow exponentially in r as $r \to \infty$, those with $\mathrm{Re}(k) > 0$ decay exponentially in r.

At the pinch point $k \approx 0.6714 - 1.809\mathrm{i}$ and $\omega \approx 1.715 - 0.2835\mathrm{i}$, implying convective instability in the axial direction because contours with $\mathrm{Im}(\omega) > 0$ cross from the upper half-plane into the lower half-plane. When S is increased, $\mathrm{Im}(\omega)$ at the pinch point increases, and the pinch point moves towards the imaginary k-axis; it crosses the imaginary k-axis at $S \approx 2.203$, and then the eigenvalues at the pinch point are $k \approx -2.245\mathrm{i}$ and $\omega \approx 2.809 - 0.2266\mathrm{i}$. Lim & Redekopp (1998) and Gallaire & Chomaz (2003*a*) do not consider this dispersion relation for $S > 2.203$ because of the difficulty of interpreting modes that cross into the left half-plane. The analytic continuation into the left half-plane is obtained by replacing $\sqrt{k^2}$ by $-\sqrt{k^2}$ in (4.7), and hence in (4.11), i.e. by considering waves that grow exponentially with radius far from the jet core: see (A 1).

However, of particular physical significance is the value of $S = 2.882$ at which the k^+ spatial branch (a branch that lies in the upper half-plane for large positive $\mathrm{Im}(\omega)$, and corresponds to a downstream-propagating wave) with $\mathrm{Im}(\omega) = 0$ touches the imaginary k-axis: see figure 2. For $S > 2.882$, k^+ spatial branches with $\mathrm{Im}(\omega) > 0$ cross into the lower-left quadrant of the complex k-plane. In Briggs' method the integration path, which is originally placed on the real k-axis, is moved so as to remain below the k^+ branch as $\mathrm{Im}(\omega)$ is reduced. The integration path then goes from $-\infty$ on the negative real k-axis on the Riemann sheet with radially decaying solutions, to the origin, then follows below, and to the left, of the $\mathrm{Im}(\omega) = 0$ contour, and therefore crosses the imaginary k-axis onto the Riemann sheet with radially growing solutions. It then re-crosses this axis back onto the Riemann sheet with radially decaying solutions in the right half-plane. The integration path would finally return to the real k-axis, but this is not possible for the dispersion relation (4.11) because the discontinuities in (4.1) generate Kelvin–Helmholtz instability at arbitrarily short scales, causing all contours to tend to infinity in the lower-right quadrant. The ill-posed nature of this initial-value

https://doi.org/10.1017/S0022112008003236 Published online by Cambridge University Press

problem caused Gallaire & Chomaz (2003*a*) to suggest that this dispersion relation might also be unreliable in its prediction of modes crossing into the left half-plane. However, this behaviour persists in a smooth-profile version of the problem: see § 5.

The physical interpretation for branches that cross into the left half-plane was first given in Healey (2006*b*), and the findings from that paper allow us to deduce the following description for disturbances to this swirling jet.

For S just larger than 2.882 the flow is convectively unstable, so one could consider the response to periodic forcing. If the forcing frequency is chosen to lie within the range of frequencies for which the k^+ branch with $\mathrm{Im}(\omega) = 0$ lies in the left half-plane, then the forced response will be a mode that grows exponentially in r for large r. However, at finite times after the forcing is switched on, this mode will only have propagated a finite radial distance. Thus a wave growing exponentially in r can, nonetheless, satisfy homogeneous boundary conditions at any given time. The radial propagation of the front of this normal mode is part of the start-up transient created when the periodic forcing is switched on, and it can be determined from a consideration of the impulse response. The standard saddle-point method for calculating the impulse response at large times can be adapted so that propagation in the crossflow direction, as well as the usual streamwise direction, can be investigated. The radial growth predicted by saddle points in the left half-plane can also be independently confirmed by numerical evaluation of the wavenumber integral along integration paths remaining on roots of the dispersion relation that decay in the radial direction. It can be shown that disturbance energy created at the edge of the jet propagates out into the free stream, and back upstream, in such a way that sustains the exponential radial growth taking place outside the jet, where there is no shear to supply energy for the growth. See Healey (2006*b*) for detailed calculations of this type for disturbances in the rotating-disk boundary layer, where spatial branches with $\mathrm{Im}(\omega) > 0$ also cross into the left half-plane.

The main difference between the rotating-disk flow and the swirling jet is that while the eigenfunction in the former is exponential outside the boundary layer, the eigenfunction outside the jet, (4.7), only behaves exponentially at large distances from the jet axis: see (A 1). At these large radii this exponential term can be combined with the complex exponential of the wavy part of the disturbance as in Healey (2006*b*):

$$\begin{aligned} p &= p_2(r)\exp \mathrm{i}(kz - \omega t) \\ &= A K_0(\sqrt{k^2}r)\exp \mathrm{i}(kz - \omega t) \\ &\sim A\left(\frac{\pi}{2\sqrt{k^2}r}\right)^{1/2} \exp \mathrm{i}(kz - \omega t + \mathrm{i}\sqrt{k^2}r). \end{aligned} \tag{4.12}$$

Saddle-point theory can then be used on this combined exponential term to describe radial propagation as well as axial propagation. The presence of the algebraic term in r in (4.12) does not affect the propagation properties at leading order.

However, this growth in the radial direction only continues until the disturbance reaches the boundary of the flow. Ordinarily, a boundary placed far from the jet has little influence on the disturbances within the jet because of their exponential radial decay outside the jet. Conversely, the boundary, however far away, has a major effect on these modes that grow exponentially in the radial direction. The effects of crossflow confinement on this type of mode were investigated in Healey (2007) for waves in a model of the rotating-disk boundary layer. The typical effect on temporal instability of moving a boundary closer to a shear layer whose modes decay in the crossflow direction is one of increasing stabilization as the boundary approaches the

https://doi.org/10.1017/S0022112008003236 Published online by Cambridge University Press

shear layer and the flow becomes more confined. However, when disturbances grow in the crossflow direction, Im(ω) at the pinch point increases when the flow is confined, regardless of how far away the confining boundary is. This will enhance the growth rate of an existing absolute instability, or can create an absolute instability where previously there was only convective instability. Furthermore, Im(ω) at the pinch point actually increases if the confining boundary is moved towards the shear layer (although there is stabilization when the flow is strongly confined).

These counter-intuitive aspects of problems with modes growing in the crossflow direction follow from an understanding of the effect of confinement on the complex-wavenumber plane. As shown below, the major effect of confinement is to replace the continuous spectrum associated with the branch-cut at the imaginary k-axis of the unconfined problem by an infinite discrete spectrum in the confined problem. This qualitative difference arises however weakly confined the flow is, and strongly affects the behaviour of the Im(ω) = 0 spatial branch shown in figure 2 where it approaches the imaginary k-axis.

4.2. *Confined flow*

We surround the swirling jet by an outer cylinder of dimensionless radius h, coaxial with the jet, giving outer boundary condition $u_2(h) = 0$, and therefore $p_2'(h) = 0$ by (4.8). The solution to (4.6) is now

$$p_2 = A'[I_1(\sqrt{k^2}h)K_0(\sqrt{k^2}r) + K_1(\sqrt{k^2}h)I_0(\sqrt{k^2}r)], \tag{4.13}$$

where A' is a constant of integration and I_m is the order-m modified Bessel function of the first kind. Substituting (4.3), (4.5), (4.8) and (4.13) into (4.9) and (4.10) and eliminating the constant A' produces the dispersion relation for axisymmetric waves in the confined swirling jet:

$$0 = k^2S^2 + \beta(\omega - k)^2\frac{J_0(\beta)}{J_1(\beta)} + \omega^2\sqrt{k^2}\frac{I_1(\sqrt{k^2}h)K_0(\sqrt{k^2}) + I_0(\sqrt{k^2})K_1(\sqrt{k^2}h)}{I_1(\sqrt{k^2}h)K_1(\sqrt{k^2}) - I_1(\sqrt{k^2})K_1(\sqrt{k^2}h)}, \tag{4.14}$$

in agreement with Lim & Redekopp (1998).

The large-argument asymptotic formulae for K_1 and I_1, (A 1) in the Appendix, show that (4.14) approaches (4.11) for large Re(k)h, i.e. away from the imaginary k-axis for large enough h. However, even when h is large, (4.14) differs substantially from (4.11) when Re(k) = $O(h^{-1})$. Therefore, confinement is a singular perturbation to the dispersion relation with significant effect close to the imaginary k-axis, and negligible effect away from the imaginary k-axis. This is why the spatial branch with Im(ω) = 0 shown in figure 2 is strongly affected by confinement, however large the radius of the outer cylinder.

We now show that the main qualitative effect of confinement is to replace the continuous spectrum associated with the branch cut at the imaginary k-axis due to the term $\sqrt{k^2}$, with an infinite discrete spectrum. Rules concerning Bessel functions, (A 2) in the Appendix, can be used to verify that (4.14) is invariant under $\sqrt{k^2} \to -\sqrt{k^2}$. Therefore, the branch cut present in the unconfined dispersion relation (4.11) is not present in the confined dispersion relation (4.14). The presence of the infinite discrete spectrum in (4.14) is most easily seen from the poles of the relation $\omega = \omega(k)$, i.e. points in the complex k-plane where $\omega \to \infty$. Spatial branches start and/or finish on such points. The poles lie on the imaginary k-axis, and can be found by letting $\omega \to \infty$, and $k = \mathrm{i}k_i$, in (4.14), which leads to

$$J_1(hk_i)\,[J_1(k_i)Y_0(k_i) - J_0(k_i)Y_1(k_i)] = 0, \tag{4.15}$$

https://doi.org/10.1017/S0022112008003236 Published online by Cambridge University Press

where Y_m is the order-m Bessel function of the second kind, and relations (A 3) from the Appendix have been used to simplify expressions. The poles created by confinement are given by the zeros of $J_1(hk_i)$, the first few of which are $hk_i \approx \pm 3.83$, ± 7.02, $\pm 10.17\ldots$. The function J_1 is oscillatory along the real axis of its argument, so there are infinitely many poles created by confinement, and they are $O(h^{-1})$ apart along the imaginary k-axis when h is large. Note that the position of the poles is independent of the swirl, S.

Healey (2007) studied the effects of confinement in a piecewise linear planar flow and found that there is a pair of branch-points connecting two Riemann surfaces of solutions $\omega = \omega(k)$ close to each pole for large h. In that problem the dispersion relation is a quadratic equation in ω, but (4.14) is a transcendental equation in ω, with the possibility of many ω solutions of (4.14) coexisting for a given value of k, i.e. many Riemann surfaces of solutions $\omega = \omega(k)$ in the complex k-plane connected by many branch-points. However, there are only a few solutions with $\mathrm{Im}(\omega) > 0$. Nonetheless, the structure of the ω solutions of (4.14), and their poles and branch-points, is still relatively complicated. Figure 3 shows graphs of $\mathrm{Im}(\omega)$ along the negative imaginary k-axis when $h = 5$. One of the ω roots of (4.14) corresponds to the surface of solutions of (4.11) shown in figure 2 as $h \to \infty$. Branch cuts could be placed along the imaginary axis of the complex k-plane between pairs of these branch points to define the extent of each Riemann surface.

The Riemann surface of $\mathrm{Im}(\omega)$ for the confined dispersion relation, (4.14), corresponding to that for the unconfined dispersion relation, (4.11), shown in figure 2, is presented in figure 4. Contours of constant $\mathrm{Im}(\omega)$ that terminate on the imaginary k-axis have encountered branch cuts (the branch cuts and branch points are not shown in this figure, but the branch points are shown in figure 3). However, the most important result is that, as in Healey (2007), there is a saddle point associated with each pole created by confinement. Some of these new saddle points in the confined flow are higher than any saddle point of the unconfined flow, and create absolute instability in the confined flow even though the unconfined flow is only convectively unstable for this value of the swirl, S. As $h \to \infty$ the poles become closer together and the confinement saddle points asymptote towards the imaginary k-axis, but some always remain in the $\mathrm{Im}(\omega) > 0$ part of the Riemann surface because the $\mathrm{Im}(\omega) = 0$ contour in the unconfined problem touches the imaginary k-axis. Therefore, the confined flow remains absolutely unstable for arbitrarily large h. The physical explanation for this behaviour at large h lies in confinement converting the radial growth and propagation of disturbances found in the unconfined problem into a standing wave once they eventually reach the outer cylinder. This mechanism is explored in more detail in Healey (2007).

The creation of absolute instability by confinement allows a neutral curve for axisymmetric absolute instability to be constructed in the (h, S)-plane and this is shown in figure 5(a). As h is varied the confinement saddle points move in the complex k-plane, and $\mathrm{Im}(\omega)$ at each saddle changes, and so dominance switches from saddle to saddle. These changes in dominance account for the series of jumps in gradient of the neutral curve for absolute instability. The absolute frequencies and wavenumbers along the neutral curve are also shown, and they asymptote towards the eigenvalues at the point where the $\mathrm{Im}(\omega) = 0$ contour touches the imaginary k-axis in the unconfined problem as $h \to \infty$ because as h increases the saddle points created by confinement asymptote towards the imaginary k-axis. As in Healey (2007), the trend is for absolute instability to increase when h is reduced until eventually h becomes small enough and then confinement exerts the stabilizing influence that it is

https://doi.org/10.1017/S0022112008003236 Published online by Cambridge University Press

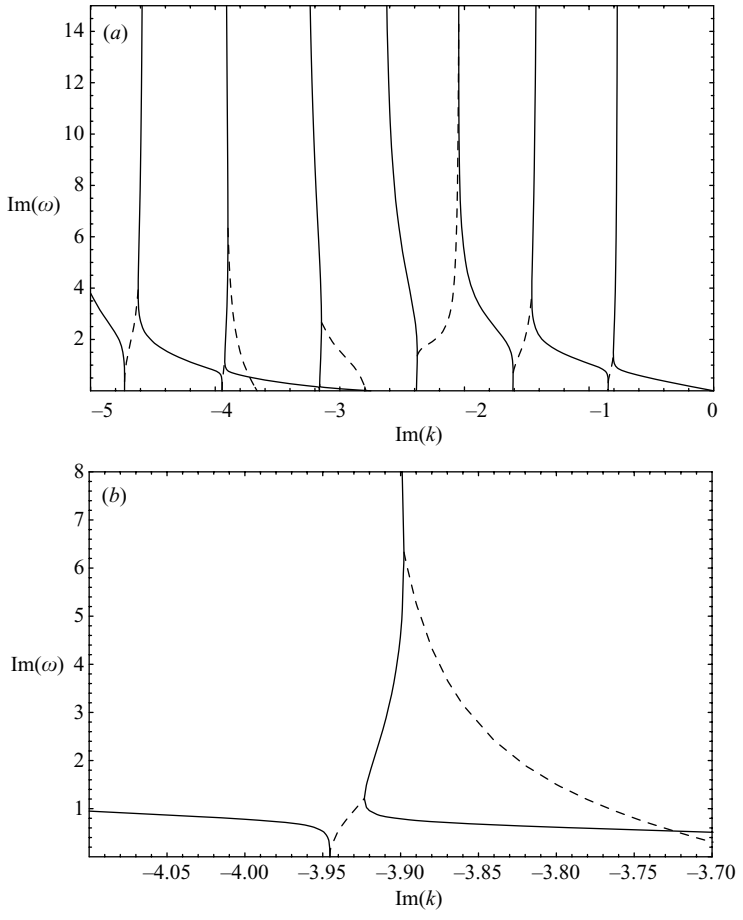


FIGURE 3. Behaviour of solutions for ω of (4.14) along the imaginary k-axis for $h = 5$. Solid lines are $\mathrm{Im}(\omega)$ for purely imaginary roots of (4.14); dashed lines are $\mathrm{Im}(\omega)$ for pairs of roots of (4.14) whose real parts have equal magnitude but are of opposite sign. The dashed lines emerge from branch points where a pair of solid lines meet. (*b*) is an enlargement of (*a*). There are up to three values of ω with $\mathrm{Im}(\omega) > 0$ satisfying (4.14) over the interval of the imaginary k-axis shown. The vertical asymptotes are the poles of $\omega = \omega(k)$, which lie at values of k that satisfy (4.15).

usually associated with. However, although even strong confinement can destabilize an absolute instability (see Juniper 2006), we shall not consider $h \to 1$ since (4.1) is not plausible in this limit (viscous effects would then be important because the boundary layer on the confining outer cylinder would interact with the jet core).

4.3. *Benjamin's criticality condition*

The supercritical–subcritical transition occurs when a dispersion relation admits solutions with zero phase velocity and zero wavenumber. Setting $\omega = 0$, and letting $k \to 0$, in either (4.11) or (4.14) leads to the same eigenrelation for the swirl, S:

$$0 = 2J_0(2S) + SJ_1(2S). \tag{4.16}$$

As the swirl increases from zero, the first root of (4.16) to be encountered is $S \approx 1.4946$. There are infinitely many roots, but this is the one with smallest positive S. For

https://doi.org/10.1017/S0022112008003236 Published online by Cambridge University Press

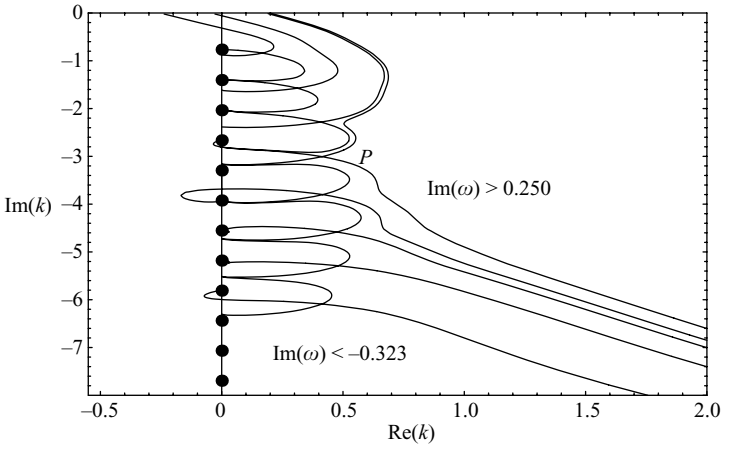


FIGURE 4. Contours of constant $\mathrm{Im}(\omega)$ in the complex k-plane for the dispersion relation for the confined jet (4.14) for $S = 2.882$ and $h = 5$. Contours are at the levels of the saddle points created by confinement; the saddles, and $\mathrm{Im}(\omega)$ for each one, in the form $(k, \mathrm{Im}(\omega))$, are at $(0.167 - 0.840\mathrm{i}, -0.319)$, $(0.312 - 1.574\mathrm{i}, -0.056)$, $(0.408 - 2.283\mathrm{i}, 0.228)$, $(0.414 - 3.01\mathrm{i}, 0.250)$, $(0.417 - 3.800\mathrm{i}, 0.171)$, $(0.475 - 4.584\mathrm{i}, 0.121)$, $(0.481 - 5.289\mathrm{i}, -0.009)$ and $(0.414 - 6.090\mathrm{i}, -0.323)$. The dominant saddle point (pinch point), marked P, lies at $(0.414 - 3.01\mathrm{i}, 0.250)$. The integration path lies in the region $\mathrm{Im}(\omega) < 0.250$, passing along the negative real k-axis to the origin, then over the saddle at P and finally following below the $\mathrm{Im}(\omega) = 0.250$ contour to the right of the diagram. The poles are marked by solid disks.

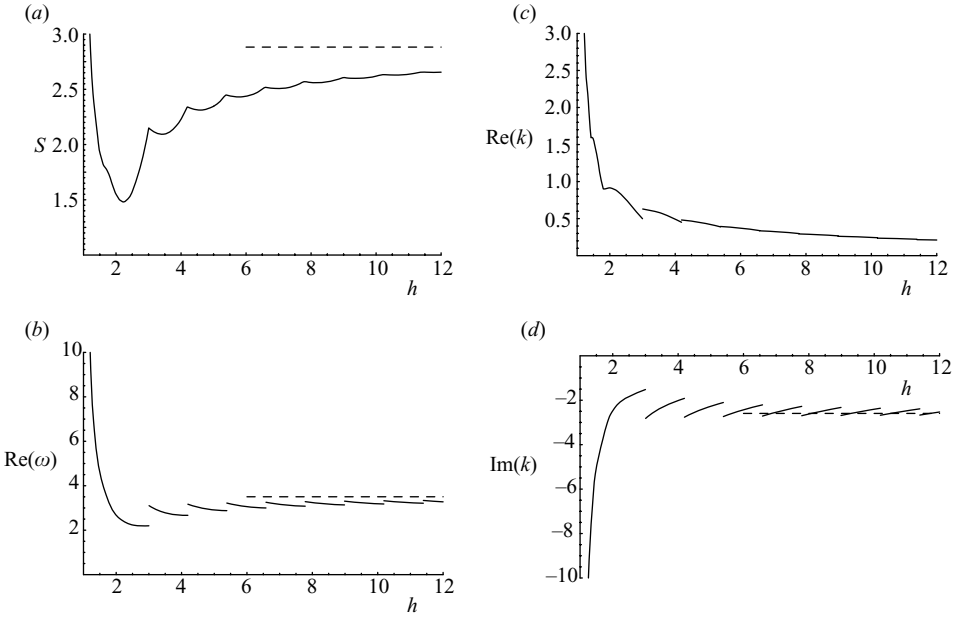


FIGURE 5. (*a*) Neutral curve for absolute instability for the confined-flow dispersion relation (4.14). (*b*)–(*d*) frequencies and wavenumbers at the pinch points along the neutral curve for absolute instability shown in (*a*); discontinuities occur at changes in dominance of the saddle points. Dashed lines indicate asymptotes of the curves as $h \to \infty$, which are obtained from the eigenvalues at the point where the $\mathrm{Im}(\omega) = 0$ contour touches the imaginary k-axis in the unconfined problem, which is at $S = 2.882$, as shown in figure 2, and this swirl provides the horizontal asymptote for the neutral curve shown in (*a*).

https://doi.org/10.1017/S0022112008003236 Published online by Cambridge University Press

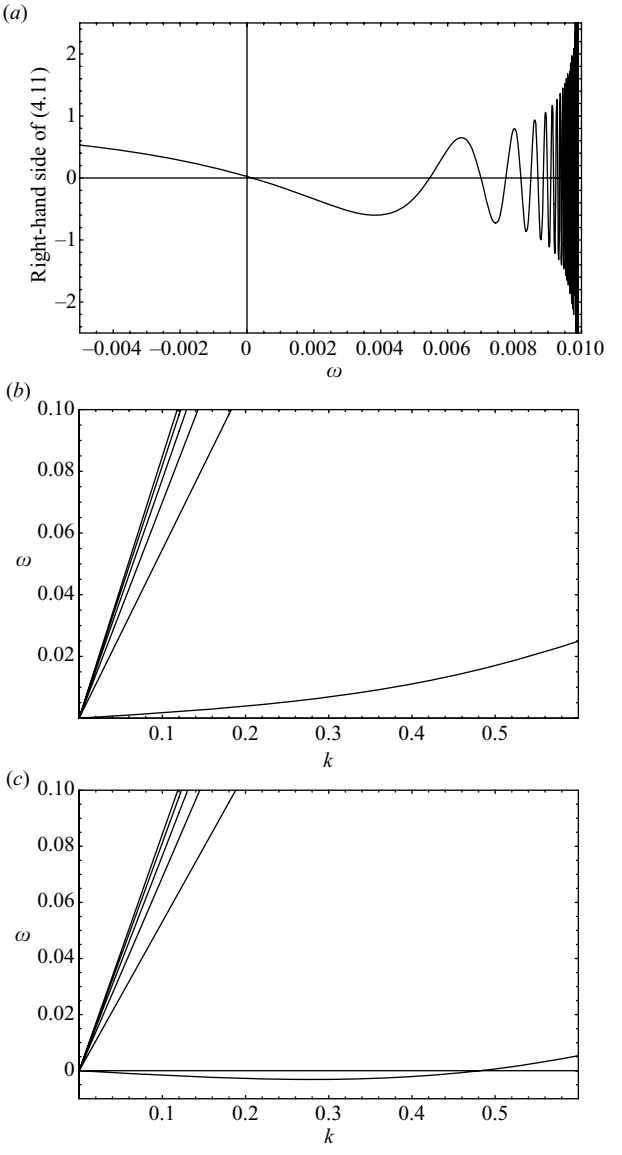


FIGURE 6. (*a*) Right-hand side of dispersion relation for unconfined swirling jet (4.11) against real frequency ω, for $k = 0.01$ and $S = 1.47$. (*b*) Dispersion relations for neutral inertial waves in slightly supercritical flow, $S = 1.47$. (*c*) Dispersion relations for neutral inertial waves in slightly subcritical flow, $S = 1.52$.

$S < 1.4946$ the flow is supercritical, and it becomes subcritical for $S > 1.4946$ for both the confined and unconfined dispersion relations.

Therefore, although the absolute instabilities of this model swirling jet depend sensitively on the nature of the confinement, Benjamin's criticality condition is independent of the confinement of this swirling jet. We wish to explore this criticality condition from the perspective of Briggs' method, and we start with some well-known observations for this type of flow.

At a given positive value of S there are infinitely many neutral inertial waves. This is illustrated in figure 6(*a*), where the right-hand side of (4.11) has been plotted as

https://doi.org/10.1017/S0022112008003236 Published online by Cambridge University Press

a function of ω for $k = 0.01$ and for a slightly supercritical value of $S = 1.47$. Every zero of this function corresponds to a neutral temporal eigenvalue, and the function oscillates around zero infinitely many times as $\omega \to k$, since then $\beta \to \infty$ by (4.4). The criticality condition, A in figure 1(*a*), is met when S is such that the curve in figure 6(*a*) passes through the origin as $k \to 0$; standing waves of axial wavelength L appear in a pipe of length L at the S for which the curve in figure 6(*a*) passes through the origin when $k = 2\pi/L$, which corresponds to B in figure 1(*a*). Therefore, $B \to A$ as $L \to \infty$. The dispersion relations for the first few of these neutral waves are shown in figure 6(*b*), which makes clear the existence of a mode with small phase velocity corresponding to the intersection of the curve with the horizontal axis near the origin in figure 6(*a*); the accumulation of modes whose phase velocity approaches unity is also apparent.

The important qualitative change that takes place when the flow becomes subcritical is shown in figure 6(*c*). The mode with small positive phase velocity in the supercritical case now has a small negative phase velocity over a finite interval of k. The finite value of $k = k_0$ where this mode has zero phase velocity gives the length of pipe, $L = 2\pi/k_0$, in which a standing wave first appears at this level of swirl, i.e. point B in figure 1(*a*). This length rapidly reduces as the swirl increases above its critical value. Similar diagrams are shown in figure 3 of Gallaire & Chomaz (2004) for the Rankine vortex with axial flow, where spatial dispersion relations, i.e. k as a function of ω, are also shown.

These neutral inertial waves can be described using a long-wave theory: substituting $\omega = c_0 k$ in (4.11) or (4.14), and considering $k \to 0$, gives at leading order

$$0 = 2J_0\left(\frac{2S}{1-c_0}\right) + \frac{S}{1-c_0}J_1\left(\frac{2S}{1-c_0}\right). \tag{4.17}$$

For example, when $S = 1.47$, the neutral inertial waves are $c_0 = 0.0165, 0.5465, 0.6998, 0.7744, 0.8189, \ldots$, in good agreement with the gradients at the origin of the curves in figure 6(*b*). However, in this long-wave limit, the unstable wave, which can give rise to absolute instability, has $c_0 = 1 + 0.6479\mathrm{i}$ at $S = 1.47$, and therefore corresponds to a branch of the dispersion relation that is distinct from the inertial waves. Benjamin's criticality condition would therefore not be seen in a study of the complex k-plane for the unstable mode, since it lies on a different Riemann surface. However, Loiseleux *et al.* (1998) found that non-axisymmetric unstable modes can resonate and interact, i.e. form branch points, with non-axisymmetric neutral inertial modes; we expect the same to occur for the flow considered here.

From the point of view of Briggs' method, however, the feature of particular interest in figure 6(*c*) is the local minimum in the dispersion relation of the mode with negative phase velocity. At this point $\mathrm{d}\omega/\mathrm{d}k = 0$ and so a saddle point exists on the real k-axis, which is not present in the dispersion relations of the supercritical flow shown in figure 6(*b*). Contours of constant $\mathrm{Im}(\omega)$ in the complex k-plane for a supercritical and subcritical level of swirl are shown in figure 7.

In the supercritical flow (figure 7*a*), the integration path can be deformed below the real k-axis into the region where $\mathrm{Im}(\omega) < 0$. Therefore, although axially periodic waves are neutrally stable, an impulsive disturbance will be carried downstream and the disturbance decays exponentially in the rest frame, as in Wang & Rusak (1996). In the subcritical flow (figure 7*b*), the integration path can be deformed into the valleys of the saddle point on the real k-axis, and passes over this saddle point, where $\mathrm{Im}(\omega) = 0$. Although this saddle is neutrally stable, saddle-point theory

https://doi.org/10.1017/S0022112008003236 Published online by Cambridge University Press

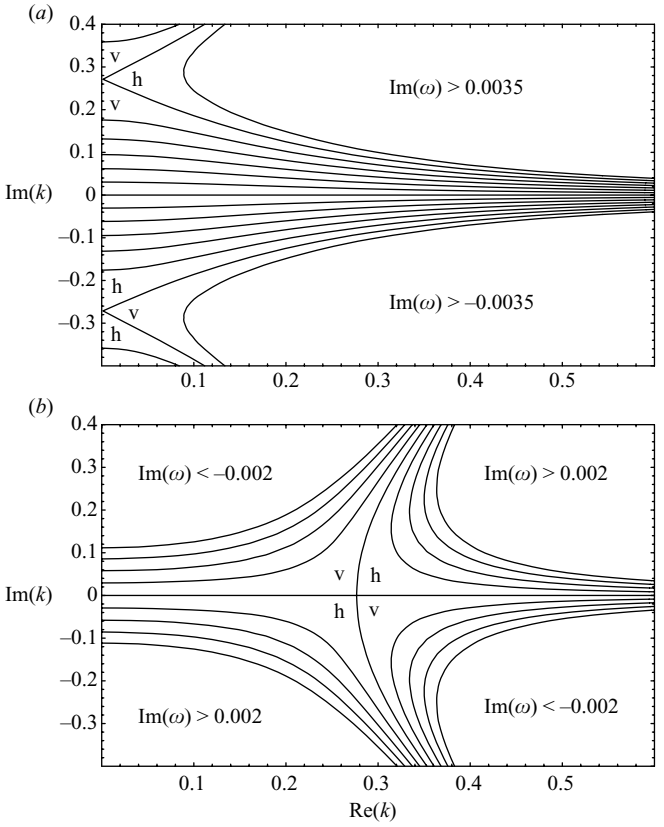


FIGURE 7. Contours of constant $\mathrm{Im}(\omega)$ in the complex k-plane for the unconfined dispersion relation (4.11) for (*a*) a supercritical flow, $S = 1.47$, and (*b*) a subcritical, $S = 1.52$. In each diagram there is an $\mathrm{Im}(\omega) = 0$ contour on the real k-axis (these are neutral waves). Valleys and hills near a saddle point are indicated by a 'v' and an 'h' respectively.

predicts that an impulsive disturbance will decay like $t^{-1/2}$, i.e. much more slowly than the exponential decay of the supercritical flow. Wang & Rusak found exponential growth in the subcritical flow in a finite-length pipe via a mechanism that depends on the interaction of disturbances with the upstream and downstream boundary conditions.

The criticality condition, $S = 1.4946$, is lower than the condition for absolute instability shown in figure 5 (except for a vary narrow range of h), so as the swirl is increased the steady transcritical bifurcation associated with criticality occurs before any unsteady bifurcation associated with the absolute instability. However, this is not always the case for the physically more realistic swirling jet models considered in the next section.

5. A model swirling jet with smooth velocity profiles

The model swirling jet velocity profiles (4.1) have discontinuities at the jet edge, and so both dispersion relations (4.11) and (4.14) predict amplification disturbances of arbitrarily short length scales by Kelvin–Helmholtz instability. This prevents the integration path in the complex-wavenumber plane from returning to the real-wavenumber axis, and makes both initial-value problems ill-posed. Absolute instability

https://doi.org/10.1017/S0022112008003236 Published online by Cambridge University Press

calculations are concerned with determining the behaviour of the initial-value problem at large times, so it might be argued that (4.1), and therefore (4.11) and (4.14), are unsuitable for such investigations, and perhaps the counter-intuitive behaviours described in § 4 are artifacts of the discontinuities in (4.1). We show in this section that this is not the case. We present stability results for smooth jet profiles that confirm that (4.1) is a good model when the shear layer at the jet edge is relatively thin, that the behaviour shown in figure 2 is reproduced in this case, and that the short-wave stabilization produced by introducing a finite-thickness shear layer at the jet edge does not alter the dominance of the saddle points. The effects of increasing the thickness of this shear layer are also investigated.

Consider the dimensionless model swirling-jet velocity profiles

$$V(r) = \frac{Sr}{2}\left[1 - \mathrm{erf}\left(\frac{r-1}{d}\right)\right], \quad W(r) = \frac{1}{2}\left[1 - \mathrm{erf}\left(\frac{r-1}{d}\right)\right], \tag{5.1a, b}$$

where

$$\mathrm{erf}(x) = \frac{2}{\sqrt{\pi}}\int_0^x \mathrm{e}^{-t^2}\,\mathrm{d}t \tag{5.2}$$

is the error function, which has the property $\lim_{x\to\pm\infty}\mathrm{erf}(x) = \pm 1$. These profiles produce shear layers of dimensionless thickness d at the edge of the jet for both axial and azimuthal profiles, and they are exponentially close to (4.1) when $|r-1|/d$ is large.

Gallaire & Chomaz (2003*b*) have also considered smooth velocity profiles that decay to zero outside the jet. Their models are more complicated and have a number of parameters that were tuned to give best fit to the experimental profiles of Billant *et al.* (1998). However, (5.1) captures the essential properties required for present purposes.

The model profiles (5.1) are substituted into (3.3), which are solved numerically with boundary conditions for unconfined flow. An advantage of these profiles is that, away from the shear layers at the jet edge, the analytic solutions (4.3) and (4.7) apply, and can be used to produce initial conditions for the numerical solution on each side of the shear layer. The linearized equations are solved by integrating (3.3) from $r = 1 - 4d$ to $r = 1$, and from $r = 1 + 4d$ to $r = 1$, and the solutions from each side of the shear layer are matched by requiring p/p' to be continuous at $r = 1$, to produce roots of the dispersion relation. To ensure the accuracy of (4.3) in providing initial conditions at $r = 1 - 4d$ we only consider $0 < d < 1/4$. There is no stiffness in the differential equations even when d is numerically small, because the integration range scales with d.

5.1. *Absolute instability of the unconfined smooth flow*

Figure 8 shows contours of constant $\mathrm{Im}(\omega)$ for basic flow (5.1) with $S = 2.846$ and $d = 0.005$. This figure confirms that the behaviour seen in figure 2 for the model profiles (4.1) also occurs for smooth continuous profiles. Both saddle points have $\mathrm{Im}(\omega) < 0$ and so the flow is not absolutely unstable. It is convectively unstable in the downstream direction, on account of the $\mathrm{Im}(\omega) = 0$ contour crossing the real k-axis from the upper half-plane into the lower half-plane. Furthermore, the flow is incipiently convectively unstable in the radial direction, on account of the $\mathrm{Im}(\omega) = 0$ contour crossing the imaginary k-axis from the right half-plane into the left half-plane for marginally increased swirl, S. However, confining the jet within a cylinder co-axial with the jet will convert this radial convective instability into an absolute instability,

https://doi.org/10.1017/S0022112008003236 Published online by Cambridge University Press

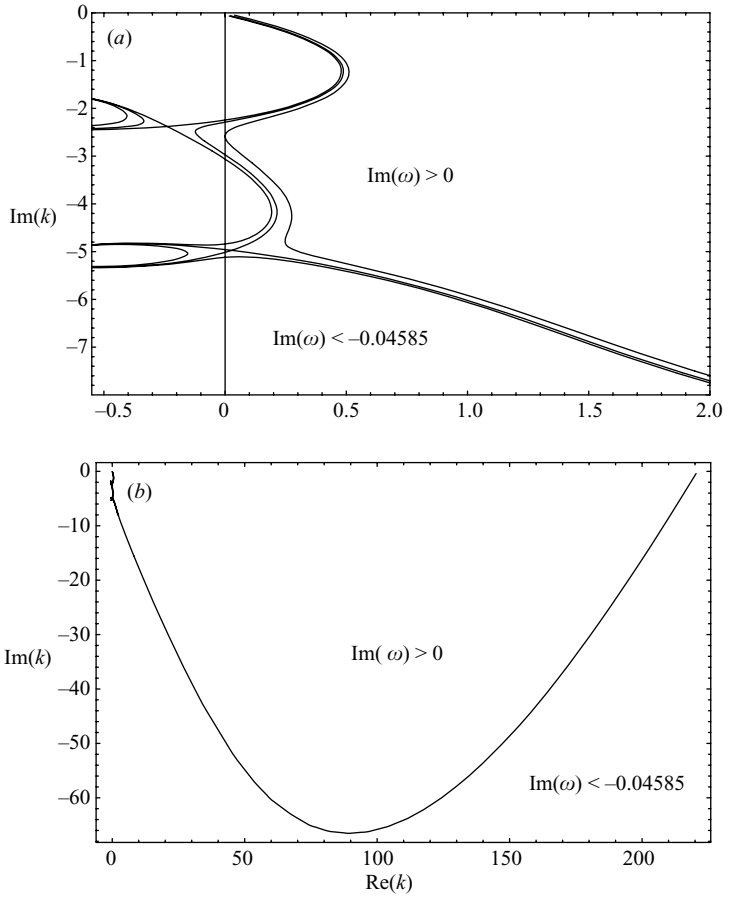


FIGURE 8. Contours of constant $\mathrm{Im}(\omega)$ in the complex k-plane for the dispersion relation for the smooth unconfined jet (5.1) for $S = 2.846$ and $d = 0.005$. Contours are at $\mathrm{Im}(\omega) = -0.04585$, -0.03313 and 0. The dominant saddle point (pinch point) lies at $k \approx 0.0281 - 4.973\mathrm{i}$, at which $\omega \approx 4.611 - 0.03313\mathrm{i}$; the other saddle point lies at $k \approx -0.2387 - 2.379\mathrm{i}$, at which $\omega \approx 3.402 - 0.04585\mathrm{i}$. The branch cut originally placed on the imaginary k-axis has been removed so that solutions with $\mathrm{Re}(k) < 0$ grow exponentially in r as $r \to \infty$, and those with $\mathrm{Re}(k) > 0$ decay exponentially in r. In (a) the integration path lies to the left of the $\mathrm{Im}(\omega) = 0$ contour, as in figure 2. A larger part of the complex k-plane is shown in (b), and the integration path lies below the $\mathrm{Im}(\omega) = 0$ contour and returns to the positive real k-axis for $\mathrm{Re}(k) > 220$ (the different contours are indistinguishable on this scale).

even when the radius of the cylinder is very large, due to the creation of additional saddle points near the imaginary k-axis, as in figure 4.

Figure 8(b) shows that the introduction of the finite thickness shear layer at the jet edge stabilizes short wavelength waves and allows the integration path to reach the positive real k-axis, thus creating a well-posed initial-value problem, in contrast to the model jet profiles (4.1). No additional saddle points with $\mathrm{Im}(\omega) > 0$ are encountered for these S and d by the introduction of the shear layer at the jet edge.

However, increasing the thickness, d, of the shear layer at the jet edge sufficiently does have a qualitative effect on the stability characteristics. Figure 9 shows the neutral curve for absolute instability when the shear layer at the jet edge is included. It is verified that the stability characteristics obtained numerically for the smooth velocity

https://doi.org/10.1017/S0022112008003236 Published online by Cambridge University Press

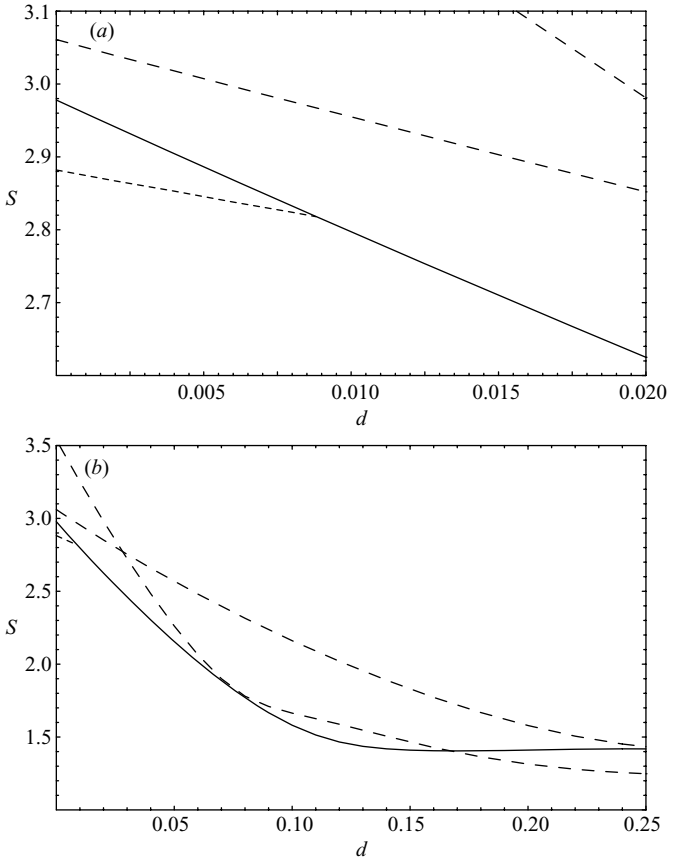


FIGURE 9. The solid line is the neutral curve for absolute instability for the smooth profiles (5.1) with unconfined flow; the line with short dashes is where the $\mathrm{Im}(\omega) = 0$ contour touches the imaginary k-axis, which indicates when the corresponding confined problem will be absolutely unstable as $h \to \infty$; lines with long dashes indicate subdominant, or irrelevant, saddle points with $\mathrm{Im}(\omega) = 0$. (*a*) is an enlargement of (*b*). Values at $d = 0$ were obtained using (4.11). Eigenvalues at the pinch points on the neutral curve are shown in figure 11.

profiles (5.1) approach those obtained analytically, (4.11), from the discontinuous profiles (4.1) as $d \to 0$. The main observation to be made is that increasing d tends to destabilize the flow. The incipient radial convective instability for $d = 0.005$ occurs at $S = 2.846$, while it occurs at 2.882 in the discontinuous model (4.1). Comparing figures 2 and 8 also shows that both saddle points have their $\mathrm{Im}(\omega)$ raised when the shear layer thickness is raised from zero to $d = 0.005$, with the saddle nearer the imaginary k-axis showing the greater increase in $\mathrm{Im}(\omega)$, and becoming dominant. These trends continue as d increases further, and for $d > 0.0088$ the flow becomes absolutely unstable, with no contours with $\mathrm{Im}(\omega)$ greater than at the dominant saddle (pinch point) crossing into the left half of the complex k-plane, i.e. a 'conventional' absolute instability. Note that when $d < 0.0088$ the flow is absolutely unstable for large enough swirl although the pinch point crosses into the left half-plane. In fact, the destabilization produced by thickening the shear layer is relatively strong. When the shear layer thickness is increased from $d = 0.01$ to $d = 0.1$, the swirl required to produced absolute instability is reduced from $S = 2.797$ to $S = 1.581$. Although

https://doi.org/10.1017/S0022112008003236 Published online by Cambridge University Press

for $d > 0.0088$ confinement is not necessary to create a conventional right half-plane absolute instability, it can still enhance the absolute instability: see § 5.2 below.

Therefore, the introduction of a finite-thickness shear layer stabilizes the short waves that arise from the Kelvin–Helmholtz instability at the jet edge, but it also destabilizes longer waves since it reduces the swirl necessary to produce absolute instability. The latter instability mechanism appears to be related to an enhancement of the centrifugal instability present in the shear layer. In the absence of mean axial shear Rayleigh's criterion applies, and the flow is centrifugally unstable where the square of the circulation decreases, and it is stable otherwise. The piecewise linear profile (4.1) is centrifugally stable everywhere, except at the jet edge where the circulation drops discontinuously to zero. Howard & Gupta (1962) have shown that with mean axial shear the square of the circulation must increase sufficiently quickly to guarantee stability (a quantity analogous to the local Richardson number of stratified flows must be greater than 1/4), but axial shear does not necessarily produce, or enhance, centrifugal instability. These stability theorems give insight into the temporal stability properties of a flow, but do not offer guidance on changes between convective and absolute instabilities. However, increasing d increases the domain over which centrifugal instability acts, and it may be that this extension of the centrifugally unstable part of the flow is responsible for the enhancement of the axisymmetric absolute instability. Increasing d would also increase the effective Taylor number in the corresponding viscous problem if the rotating core of the jet is treated like the rotating inner cylinder, and the stationary outer fluid is treated like the fixed outer cylinder, of a Taylor–Couette experiment (again, an increase in Taylor number makes no definite prediction concerning changes in absolute instability).

5.2. *Benjamin's criticality condition for the smooth flow*

The numerical procedure for obtaining eigenvalues for the smooth profiles (5.1) is adapted for working in the limit $k \to 0$ so that Benjamin's criticality condition for the supercritical-subcritical transition can be calculated. We substitute

$$u(r) = ku_0(r), \quad v(r) = v_0(r), \quad w(r) = w_0(r), \quad p(r) = p_0(r), \quad \omega = 0 \tag{5.3}$$

into (3.3) and equate leading-order powers of k to give

$$u_0' + \frac{u_0}{r} + \mathrm{i}w_0 = 0, \tag{5.4a}$$

$$-\frac{2V}{r}v_0 = -p_0', \tag{5.4b}$$

$$\mathrm{i}Wv_0 + V'u_0 + \frac{V}{r}u_0 = 0, \tag{5.4c}$$

$$\mathrm{i}Ww_0 + W'u_0 = -\mathrm{i}p_0. \tag{5.4d}$$

Eliminating u_0, v_0 and w_0 from (5.4) gives

$$r^2W^2V(V + rV')p_0'' - rW^2[r^2VV'' + (rV')^2 - 3V^2]p_0' + 2V^2(V + rV')^2p_0 = 0. \tag{5.5}$$

There is a critical point of (5.5) at $r = r_c$ where $V(r_c) + r_cV'(r_c) = 0$. The critical point for (5.1a) lies at $r_c \sim 1 - d\sqrt{-\ln(2\sqrt{\pi}d)}$ for small d. Close to this point the two independent solutions of (5.5) are regular, and are of the form $p_0 = 1 + O(r - r_c)^3$ and $p_0 = (r - r_c)^2 + O(r - r_c)^3$. Equation (5.5) is integrated from $r = 1 - 4d$ (using initial conditions provided by (4.3)) to $r = r_c - d/10$, then from $r = r_c + d/10$ to $r = 1 + 4d$ with $p_0(r_c + d/10) = p_0(r_c - d/10)$ and $p_0'(r_c + d/10) = -p_0'(r_c - d/10)$ so that the quadratic behaviour of p_0 near $r = r_c$, with $p_0'(r_c) = 0$, is exploited. At a given value

https://doi.org/10.1017/S0022112008003236 Published online by Cambridge University Press

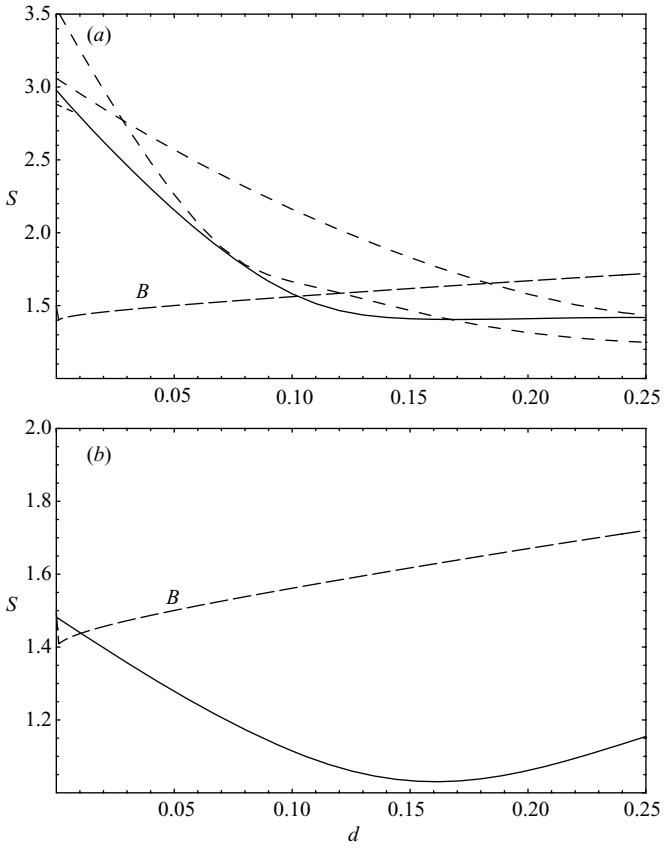


FIGURE 10. The solid line is the neutral curve for absolute instability for the smooth profiles, (5.1); the dashed line B shows Benjamin's supercritical–subcritical transition; other dashed lines are as in figure 9. (a) is for unconfined flow, (b) is for confined flow with $h = 2.2$. Discontinuous model profiles, (4.1), give Benjamin's criticality condition at $S = 1.4946$, while for the smooth profiles, (5.1), criticality is at $S = 1.4025$ at $d = 0.001$.

of d, the swirl, S, is iterated until $p_0'(1 + 4d) = 0$ to within some tolerance. We find that this value of S causes p_0 to drop rapidly to zero outside the shear layer. This is in contrast to the behaviour of the outer solution (4.1) of the discontinuous profile, which decays very slowly with increasing r as $k \to 0$. This difference between the behaviour of the solution of the smooth model and the discontinuous model leads to a small finite difference in swirl at criticality between the smooth profile as $d \to 0$ and the discontinuous profile (see caption to figure 10). However, the rapid decay of the solution outside the shear layer means that, as with the discontinuous profile, Benjamin's criticality condition for the smooth profile is independent of whether the flow is radially confined or not.

Figure 10 shows Benjamin's criticality condition and the neutral curve for absolute instability for the smooth model swirling jet (5.1). In the unconfined flow the supercritical–subcritical transition occurs at lower swirl than the absolute instability for $d < 0.1024$ and the absolute instability occurs at lower swirl for $d > 0.1024$. Figure 5 shows how confinement destabilizes the absolute instability for the discontinuous profiles, and that the strongest destabilization occurs near $h = 2.2$. Figure 10(b) shows that this confinement is also strongly destabilizing for the smooth profiles, and causes

https://doi.org/10.1017/S0022112008003236 Published online by Cambridge University Press

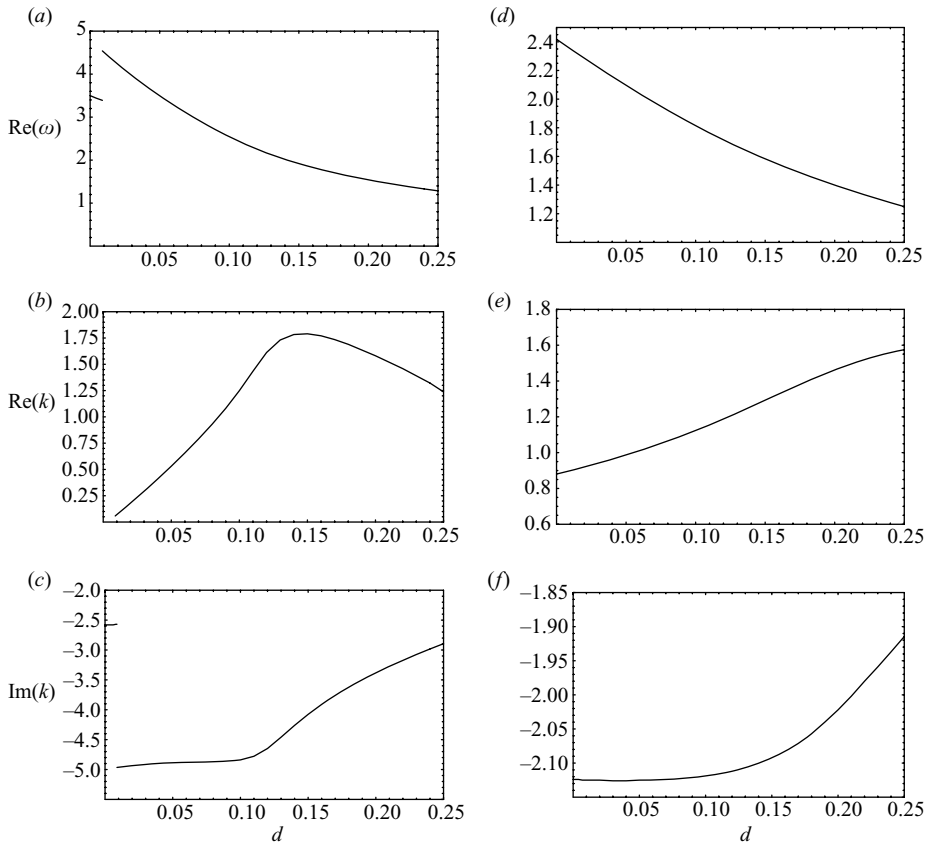


FIGURE 11. Frequencies and wavenumbers at pinch points along neutral curves for absolute instability for the smooth profiles, (5.1). (*a*)–(*c*) are for the neutral curve for the unconfined problem shown in figure 10(*a*); the eigenvalues to the left of the discontinuities correspond to those at the point where the $\mathrm{Im}(\omega) = 0$ contour touches the imaginary k-axis, as in figure 8(*a*). (*d*)–(*f*) are for the neutral curve for the confined flow with $h = 2.2$ shown in figure 10(*b*).

Benjamin's criticality condition to dominate only for $d < 0.0105$, while the absolute instability dominates for $d > 0.0105$.

The dependence of the eigenvalues at the pinch-point along the neutral curves for absolute instability on the thickness of the shear layer at the edge of the jet is shown in figure 11.

6. Conclusions

The spatio-temporal linear stability characteristics of axisymmetric disturbances to model swirling-jet velocity profiles in the inviscid limit have been investigated. The swirl at the convective–absolute transition is compared to the swirl at the supercritical–subcritical transition. A discontinuous-model swirling jet of Lim & Redekopp (1998), (4.1), for which an analytic dispersion relation can be derived, (4.11), has been re-examined. Particular attention has been paid to the crossing of the pinch point from the right half of the complex-wavenumber plane into the left half-plane. The results of Healey (2006*b*) and Healey (2007) have been used to provide a physical interpretation for this behaviour in the wavenumber plane. The presence of spatial

https://doi.org/10.1017/S0022112008003236 Published online by Cambridge University Press

branches with $\mathrm{Im}(\omega) > 0$ crossing into the left half-plane indicates propagation and exponential growth in the radial direction for large times in the unconfined flow. If the flow is radially confined, by surrounding the jet with an outer cylinder coaxial with the jet, then additional saddle points are created near the imaginary axis of the complex-wavenumber plane, and these can create absolute instability, or enhance existing absolute instability. This can take place however large the radius of the outer cylinder. Physically, the waves propagate radially outwards as in the unconfined flow until they reach the confining outer cylinder, and then they set up absolutely unstable standing waves. Neutral curves for axisymmetric absolute instability in swirling jets confined by an outer cylinder have been obtained using the analytical dispersion relation for the confined jet, (4.14).

These results for the model (4.1) are open to the criticism that the basic flow does not lead to a well-posed initial-value problem because the discontinuities produce Kelvin–Helmholtz instability at arbitrarily short length scales, and the absolute–convective stability calculations involve determining the response to an initial-value problem at large times. This issue has been addressed by presenting results for a family of smooth velocity profiles, (5.1), obtained by numerical integration of the inviscid linearized stability equations. These profiles produce a well-posed initial-value problem, and the numerical stability results confirm those of the discontinuous model. Furthermore, they reveal the role of centrifugal instability in driving the absolute instability of axisymmetric waves.

Centrifugal instability acts in the shear layer at the edge of the jet, and is found to enhance the absolute instability as the shear layer thickens due to the associated radial extension of the centrifugally unstable region. Loiseleux *et al.* (2000) also found that centrifugal instability leads to axisymmetric absolute instability, though in a less physical model swirling jet. Indeed, centrifugal instability may be essential in creating axisymmetric absolute instability. Previous spatio-temporal studies of swirling jets that found no axisymmetric absolute instability were for model jets that have no centrifugal instability: Loiseleux *et al.* (1998) considered the Rankine vortex with axial flow; Delbende *et al.* (1998) and Olendraru *et al.* (1999) considered the Batchelor vortex. Both of these flows have an outer potential vortex and the circulation increases monotonically with radius. Gallaire & Chomaz (2003*b*) have investigated the stability of profiles that do decay to zero outside the jet, and so are susceptible to centrifugal instability. Their results are restricted to $S < 1.6$, which is appropriate to the 'pre-breakdown' state, and they too found that centrifugal instability enhances absolute instability. However, they did not find axisymmetric absolute instability. They used Delbende *et al.* (1998)'s method based on direct numerical simulation of impulsive disturbances using linearized equations, which requires $\mathrm{Re}(k)$ to be sufficiently large for the axisymmetric waves to decay radially within the computational domain. The results in the present paper reveal the importance of waves with small $\mathrm{Re}(k)$ in axisymmetric absolute instability. Delbende *et al.* (1998)'s method would be better suited to the study of swirling jets confined within pipes.

The following scenario can therefore be envisaged: in an experiment on a swirling jet issuing from a nozzle at relatively large Reynolds numbers, the jet will have a thin shear layer at its edge, whose thickness will increase with downstream distance by viscous diffusion. The dependence of the jet's swirl on the downstream distance will be weaker (viscosity acts more strongly in thin layers), so to a first approximation the swirl will be constant. Figure 9 suggests, therefore, that for $1.5 < S < 2.98$ the jet will be convectively unstable as it leaves the nozzle, it will remain convectively unstable

https://doi.org/10.1017/S0022112008003236 Published online by Cambridge University Press

for some distance downstream, until the shear layer reaches a critical thickness, at which point the jet becomes absolutely unstable to axisymmetric waves.

A location where the flow undergoes a transition from convective to absolute instability provides a site for the appearance of a steep-fronted nonlinear global mode according to Couairon & Chomaz (1999) and Pier *et al.* (2001). The absolute instability frequency at this transition point drives the frequency of the global mode (the transition region acts as a wavemaker) and the imaginary part of the absolute instability wavenumber determines the spatial amplification of the front. Such modes could be related to the appearance of unsteady vortex breakdown. In contrast, the supercritical-subcritical transition of Benjamin involves waves of zero frequency and zero wavenumber and is associated with steady bifurcations leading to steady vortex breakdown. Benjamin's criticality condition has been shown to be independent of whether the flow is confined or unconfined in the radial direction, but the absolute instability has been shown to be sensitive to the confinement, with confinement creating absolute instability in the case of the discontinuous profiles, (4.1), and enhancing absolute instability in the case of the smooth profiles, (5.1). In the discontinuous profiles Benjamin's criticality condition occurs at lower swirl than the absolute instability: see § 4.3. In the unconfined smooth profiles, with shear layer thickness d (based on jet radius), the absolute instability occurs at lower swirl than Benjamin's criticality for $d > 0.1024$: see figure 10(a). In the confined smooth profile the absolute instability occurs at lower swirl than Benjamin's criticality for $d > 0.0105$ when $h = 2.2$: see figure 10(b).

It is therefore possible to have subcritical flows that are convectively unstable, and supercritical flows that are absolutely unstable.

Early authors made a strong distinction between theories for vortex breakdown based on hydrodynamic instability of a basic flow, and theories based on it being due to a change in criticality of the flow. Experimental (and numerical) evidence presented in favour of vortex breakdown being a criticality phenomenon is that its sharp onset is very much in contrast to instabilities in other shear flows, which tend to produce relatively weak streamwise amplification. However, as argued in the Introduction, the theory of absolute and convective instabilities incorporates both instability and propagation characteristics, i.e. the principal components of what had been considered to be rival theories. The steep-fronted nonlinear global mode theory of Couairon & Chomaz (1999) and Pier *et al.* (2001) predicts a sharp onset of a fully nonlinear state at a location where the flow becomes absolutely unstable, so this could be consistent with an unsteady vortex breakdown produced by absolute instability. (Weak streamwise amplification in shear layers is in fact typical of convectively unstable flows, but not necessarily of absolutely unstable flows.)

There is experimental and numerical evidence for unsteady vortex breakdown. The experiments of Escudier (1984), where a swirling jet is created in a closed cylinder with a rotating endwall, show periodically oscillating vortex breakdown at high Reynolds numbers. The axisymmetric numerical simulations of Ruith *et al.* (2003) also show oscillating axisymmetric vortex breakdown at higher Reynolds numbers, though this is overwhelmed by non-axisymmetric secondary instabilities when the non-axisymmetric terms are re-introduced. Lopez (1994) found numerically an unsteady axisymmetric branch of vortex breakdown solutions at high enough swirl; these periodic solutions are lost at a limit point as the swirl is reduced. Unsteady axisymmetric vortex breakdown was observed in the experiments of Liang & Maxworthy (2005) at swirls just below that at which a steady non-axisymmetric breakdown occurred. They also noted that a small modification to the mean flow (produced by using an alternative

https://doi.org/10.1017/S0022112008003236 Published online by Cambridge University Press

method for generating swirl in the jet) had a significant effect on the critical swirl required for breakdown. Our studies suggest that the convective–absolute transition, which may cause axisymmetric unsteady breakdown, also depends sensitively on the details of the mean velocity profiles.

Leibovich (1983) has argued that vortex breakdown is an essentially inviscid phenomenon, and Spall, Gatski & Grosch (1987) have found that a critical swirl for the onset of vortex breakdown that correlates well with experimental results for a range of swirling flows with uniform density is $S > S_{crit} = 1.67 \pm 0.08$. We have presented parameter ranges for flows where either the supercritical–subcritical transition (steady vortex breakdown) or the convective–absolute instability transition (possible unsteady vortex breakdown) can occur in inviscid flows as the swirl is increased. However, the preceding discussion of unsteady vortex breakdown highlights the importance of both Reynolds number and swirl in the selection of steady or unsteady vortex breakdown. The discussion in § 2.1 shows the qualitative changes that can occur to the steady bifurcations when viscosity is included, and also the difficulties that can exist in relating inviscid theories to numerical and experimental studies at finite Reynolds numbers. Some qualitative differences in the unsteady solutions may also be present between viscous and inviscid versions of the theory.

In the inviscid theory presented here, the columnar basic state is an exact solution and the transition to absolute instability with increasing swirl is expected to correspond to a Hopf bifurcation; nonlinear terms may either lead to a saturated stable limit cycle or further destabilize the flow. The Hopf bifurcation can sit either to the left, or to the right, of A on branch I/V in figure 1(*a*). At the codimension-two points where the criticality condition coincides with the onset of absolute instability in figure 10, the Hopf bifurcation occurs at A. The nonlinear interaction between steady and unsteady bifurcations can lead to rich dynamical behaviour, as found, for example, by Healey *et al.* (1991) in another context. In the viscous version, the basic state evolves in the axial direction and the transition from convective to absolute instability can occur at a particular axial location. As discussed above, this can be the position where a steep-fronted global mode originates, and would correspond to a limit point of periodic solutions, as found by Lopez (1994). These periodic solutions might still be traced back to a Hopf bifurcation from a steady solution branch in figure 1(*b*). Again, there may be dynamically significant codimension-two points where these Hopf bifurcations interact with limit points of steady solution branches. An extension of the present work including viscous and nonlinear effects would be required in order to investigate these issues.

Appendix. Some properties of Bessel functions

In this Appendix x has positive real part. The large-argument expansions for K_n and I_1 when the real part of x is large are

$$K_n(x) \sim \left(\frac{\pi}{2x}\right)^{1/2} \mathrm{e}^{-x}, \tag{A 1a}$$

$$I_1(x) \sim \left(\frac{1}{2\pi x}\right)^{1/2} \mathrm{e}^{x}. \tag{A 1b}$$

Changing the signs of arguments of Bessel functions gives

$$J_0(-x) = J_0(x), \quad J_1(-x) = -J_1(x), \tag{A 2a, b}$$

https://doi.org/10.1017/S0022112008003236 Published online by Cambridge University Press

$$I_0(-x) = I_0(x), \quad I_1(-x) = -I_1(x), \tag{A 2c,d}$$

$$K_0(-x) = K_0(x) - \mathrm{i}\pi I_0(x), \quad K_1(-x) = -K_1(x) - \mathrm{i}\pi I_1(x), \tag{A 2e,f}$$

and multiplying the argument by i gives

$$I_0(\mathrm{i}x) = J_0(x), \quad I_1(\mathrm{i}x) = \mathrm{i}J_1(x), \tag{A 3a,b}$$

$$K_0(\mathrm{i}x) = -\frac{\pi}{2}Y_0(x) - \mathrm{i}\frac{\pi}{2}J_0(x), \quad K_1(\mathrm{i}x) = -\frac{\pi}{2}J_1(x) + \mathrm{i}\frac{\pi}{2}Y_1(x). \tag{A 3c,d}$$

REFERENCES

Batchelor, G. K. 1964 Axial flow in trailing line vortices. *J. Fluid Mech.* **20**, 645–658.

Benjamin, T. B. 1962 Theory of the vortex breakdown phenomenon. *J. Fluid Mech.* **14**, 593–629.

Benjamin, T. B. 1967 Some developments in the theory of vortex breakdown. *J. Fluid Mech.* **28**, 65–84.

Benjamin, T. B. 1978 Bifurcation phenomena in steady flows of a viscous fluid I. Theory. *Proc. R. Soc. Lond.* A **359**, 1–26.

Benjamin, T. B. & Mullin, T. 1981 Anomalous modes in the Taylor experiment. *Proc. R. Soc. Lond.* A **377**, 221–249.

Beran, P. S. & Culick, F. E. C. 1992 The role of non-uniqueness in the development of vortex breakdown in tubes. *J. Fluid Mech.* **242**, 491–527.

Billant, P., Chomaz, J.-M. & Huerre, P. 1998 Experimental study of vortex breakdown in swirling jets. *J. Fluid Mech.* **376**, 183–219.

Briggs, R. J. 1964 *Electron-Stream Interaction with Plasmas.* MIT Press.

Couairon, A. & Chomaz, J.-M. 1999 Fully nonlinear global modes in slowly varying flows. *Phys. Fluids* **11**, 3688–3703.

Delbende, I., Chomaz, J.-M. & Huerre, P. 1998 Absolute/convective instabilities in the Batchelor vortex: A numerical study of the linear impulse response. *J. Fluid Mech.* **355**, 229–254.

Drazin, P. G. & Reid, W. H. 1981 *Hydrodynamic Stability Theory*. Cambridge University Press.

Escudier, M. P. 1984 Observations of the flow produced in a cylindrical container by a rotating endwall. *Exp. Fluids* **2**, 189–196.

Escudier, M. P., Bornstein, J. & Maxworthy, T. 1982 The dynamics of confined vortices. *Proc. R. Soc. Lond.* A **382**, 335–360.

Gallaire, F. & Chomaz, J.-M. 2003*a* Instability mechanisms in swirling flows. *Phys. Fluids* **15**, 2622–2639.

Gallaire, F. & Chomaz, J.-M. 2003*b* Mode selection in swirling jet experiments: A linear stability analysis. *J. Fluid Mech.* **494**, 223–253.

Gallaire, F. & Chomaz, J.-M. 2004 The role of boundary conditions in a simple model of incipient vortex breakdown. *Phys. Fluids* **16**, 274–286.

Gallaire, F., Ruith, M., Meiburg, E., Chomaz, J.-M. & Huerre, P. 2006 Spiral vortex breakdown as a global mode. *J. Fluid Mech.* **549**, 71–80.

Gaster, M. 1968 Growth of disturbances in both space and time. *Phys. Fluids* **11**, 723–727.

Grabowski, W. & Berger, S. 1976 Solutions of the Navier–Stokes equations for vortex breakdown. *J. Fluid Mech.* **75**, 525–544.

Harvey, J. K. 1960 Analysis of the vortex breakdown phenomenon. Part II. *Report no. 103,* Aero. Dept., Imperial College.

Harvey, J. K. 1962 Some observations of the vortex breakdown phenomenon. *J. Fluid Mech.* **14**, 585–592.

Healey, J. J. 2005 Long-wave theory for a new convective instability with exponential growth normal to the wall. *Phil. Trans. R. Soc. Lond.* A **363**, 1119–1130.

Healey, J. J. 2006*a* Inviscid long-wave theory for the absolute instability of the rotating-disk boundary layer. *Proc. R. Soc. Lond.* A **462**, 1467–1492.

Healey, J. J. 2006*b* A new type of convective instability with exponential growth perpendicular to the basic flow. *J. Fluid Mech.* **560**, 279–310.

Healey, J. J. 2007 Enhancing the absolute instability of a boundary layer by adding a far-away plate. *J. Fluid Mech.* **579**, 29–61.

https://doi.org/10.1017/S0022112008003236 Published online by Cambridge University Press

Healey, J. J., Broomhead, D. S., Cliffe, K. A., Jones, R. & Mullin, T. 1991 The origins of chaos in a modified van der Pol oscillator. *Physica* D **48**, 322–339.

Howard, L. N. & Gupta, A. S. 1962 On the hydrodynamic and hydromagnetic stability of swirling flows. *J. Fluid Mech.* **14**, 463–476.

Huerre, P. & Monkewitz, P. A. 1985 Absolute and convective instabilities in free shear layers. *J. Fluid Mech.* **159**, 151–168.

Huerre, P. & Monkewitz, P. A. 1990 Local and global instabilities in spatially developing flows. *Ann. Rev. Fluid Mech.* **22**, 473–537.

Ivanic, T., Foucault, E. & Pecheux, J. 2003 Dynamics of swirling jet flows. *Exps. Fluids* **35**, 317–324.

Juniper, M. P. 2006 The effect of confinement on the stability of two-dimensional shear flows. *J. Fluid Mech.* **565**, 171–195.

Juniper, M. P. 2007 The full impulse response of two-dimensional jet/wake flows and implications for confinement. *J. Fluid Mech.* **590**, 163–185.

Juniper, M. P. & Candel, S. M. 2003 The stability of ducted compound flows and consequences for the geometry of coaxial injectors. *J. Fluid Mech.* **482**, 257–269.

Leibovich, S. 1983 Vortex stability and breakdown: Survey and extension. *AIAA J.* **22**, 1192–1206.

Leibovich, S. & Kribus, A. 1990 Large-amplitude wavetrains and solitary waves in vortices. *J. Fluid Mech.* **216**, 459–504.

Liang, H. & Maxworthy, T. 2005 An experimental investigation of swirling jets. *J. Fluid Mech.* **525**, 115–159.

Lim, D. W. & Redekopp, L. G. 1998 Absolute instability conditions for variable density, swirling jet flows. *Eur. J. Mech.* B *Fluids* **17**, 165–185.

Loiseleux, T., Chomaz, J.-M. & Huerre, P. 1998 The effect of swirl on jets and wakes: Linear instability of the Rankine vortex with axial flow. *Phys. Fluids* **10**, 1120–1134.

Loiseleux, T., Delbende, I. & Huerre, P. 2000 Absolute and convective instabilities of a swirling jet/wake shear layer. *Phys. Fluids* **12**, 375–380.

Lopez, J. M. 1994 On the bifurcation structure of axisymmetric vortex breakdown in a constricted pipe. *Phys. Fluids* **6**, 3683–3693.

Monkewitz, P. A. & Sohn, K. D. 1988 Absolute instability in hot jets. *AIAA J.* **26**, 911–916.

Olendraru, C., Sellier, A., Rossi, M. & Huerre, P. 1999 Inviscid instability of the Batchelor vortex: Absolute–convective transition and spatial branches. *Phys. Fluids* **11**, 1805–1820.

Pier, B., Huerre, P. & Chomaz, J.-M. 2001 Bifurcation to fully nonlinear synchronized structures in slowly varying media. *Physica* D **148**, 49–96.

Ruith, M. R., Chen, P., Meiburg, E. & Maxworthy, T. 2003 Three-dimensional vortex breakdown in swirling jets and wakes: direct numerical solution. *J. Fluid Mech.* **486**, 331–378.

Sarpkaya, T. 1971 On stationary and travelling vortex breakdowns. *J. Fluid Mech.* **45**, 545–559.

Spall, R. E., Gatski, T. B. & Grosch, C. E. 1987 A criterion for vortex breakdown. *Phys. Fluids* **30**, 3434–3440.

Squire, H. B. 1956 Rotating fluids. In *Surveys in Mechanics* (ed. G. K. Batchelor & R. M. Davies), pp. 139–161. Cambridge University Press.

Squire, H. B. 1960 Analysis of the vortex breakdown phenomenon. *In Miszallaneen der Angewandten Mechanik*, pp. 306–312. Berlin: Akademie.

Tsai, C.-Y. & Widnall, S. E. 1980 Examination of a group-velocity criterion for breakdown of vortex flow in a divergent duct. *Phys. Fluids* **23**, 864–870.

Wang, S. & Rusak, Z. 1996 On the stability of an axisymmetric rotating flow in a pipe. *Phys. Fluids* **8**, 1007–1016.

Wang, S. & Rusak, Z. 1997*a* The effect of slight viscosity on a near-critical swirling flow in a pipe. *Phys. Fluids* **9**, 1914–1927.

Wang, S. & Rusak, Z. 1997*b* The dynamics of a swirling flow in a pipe and transition to axisymmetric vortex breakdown. *J. Fluid Mech.* **340**, 177–223.

Yu, M.-H. & Monkewitz, P. A. 1990 The effect of nonuniform density on the absolute instability of two-dimensional inertial jets and wakes. *Phys. Fluids* A **2**, 1175–1181.

https://doi.org/10.1017/S0022112008003236 Published online by Cambridge University Press